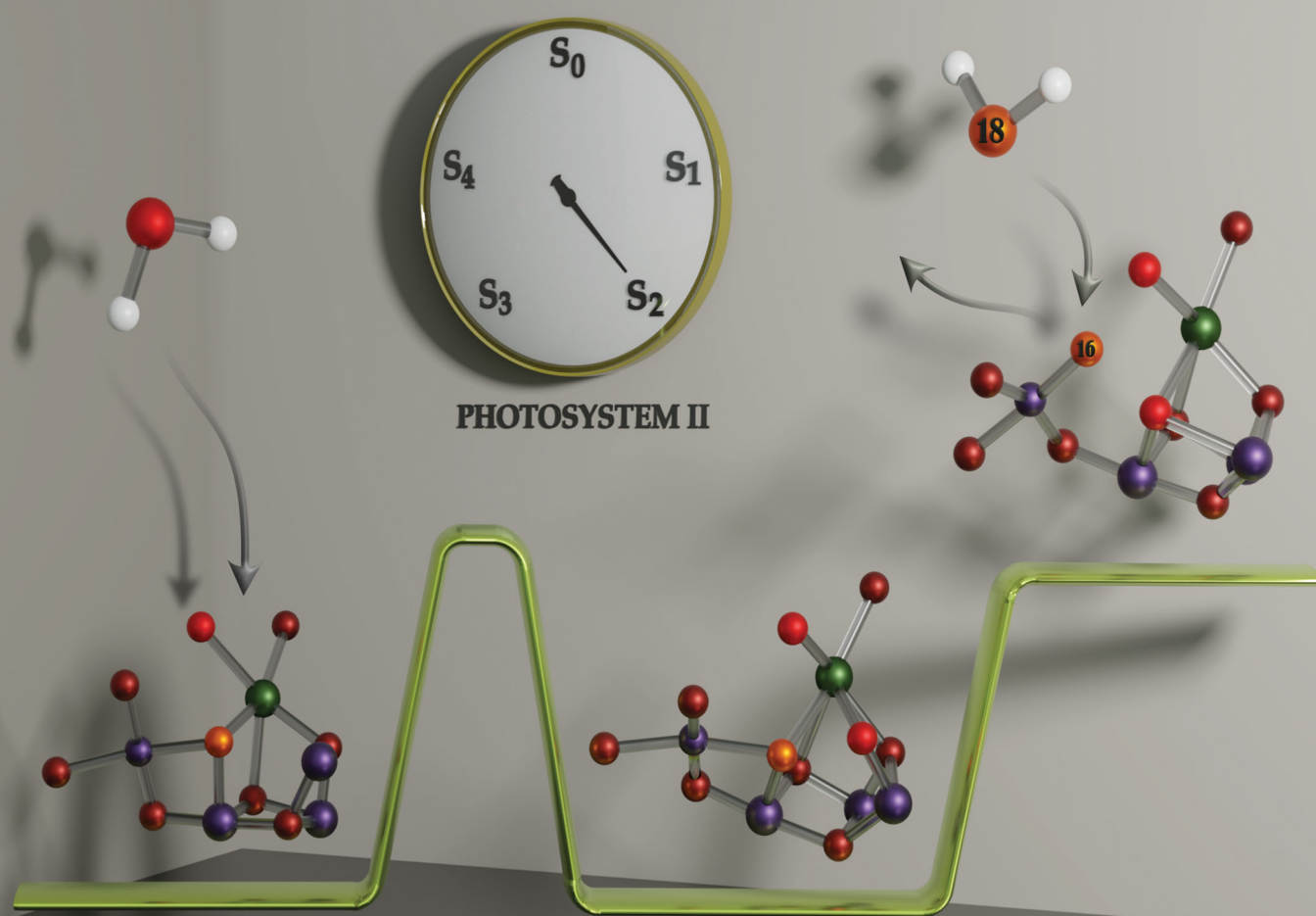


# PCCP

Physical Chemistry Chemical Physics

rsc.li/pccp



ISSN 1463-9076



## PAPER

Casper de Lichtenberg and Johannes Messinger  
Substrate water exchange in the S<sub>2</sub> state of photosystem II is  
dependent on the conformation of the Mn<sub>4</sub>Ca cluster



Cite this: *Phys. Chem. Chem. Phys.*,  
2020, 22, 12894

# Substrate water exchange in the $S_2$ state of photosystem II is dependent on the conformation of the $Mn_4Ca$ cluster

Casper de Lichtenberg <sup>a</sup> and Johannes Messinger <sup>\*ab</sup>

In photosynthesis, dioxygen formation from water is catalyzed by the oxygen evolving complex (OEC) in Photosystem II (PSII) that harbours the  $Mn_4Ca$  cluster. During catalysis, the OEC cycles through five redox states,  $S_0$  to  $S_4$ . In the  $S_2$  state, the  $Mn_4Ca$  cluster can exist in two conformations, which are signified by the low-spin (LS)  $g = 2$  EPR multiline signal and the high-spin (HS)  $g = 4.1$  EPR signal. Here, we employed time-resolved membrane inlet mass spectrometry to measure the kinetics of  $H_2^{18}O/H_2^{16}O$  exchange between bulk water and the two substrate waters bound at the  $Mn_4Ca$  cluster in the  $S_2^{LS}$ ,  $S_2^{HS}$ , and the  $S_3$  states in both Ca-PSII and Sr-PSII core complexes from *T. elongatus*. We found that the slowly exchanging substrate water exchanges 10 times faster in the  $S_2^{HS}$  than in the  $S_2^{LS}$  state, and that the  $S_2^{LS} \rightarrow S_2^{HS}$  conversion has at physiological temperature an activation barrier of  $17 \pm 1$  kcal mol<sup>-1</sup>. Of the presently suggested  $S_2^{HS}$  models, our findings are best in agreement with a water exchange pathway involving a  $S_2^{HS}$  state that has an open cubane structure with a hydroxide bound between Ca and Mn1. We also show that water exchange in the  $S_3$  state is governed by a different equilibrium than in  $S_2$ , and that the exchange of the fast substrate water in the  $S_2$  state is unaffected by Ca/Sr substitution. These findings support that (i) O5 is the slowly exchanging substrate water, with W2 being the only other option, and (ii) either W2 or W3 is the fast exchanging substrate. The three remaining possibilities for O–O bond formation in PSII are discussed.

Received 11th March 2020,  
Accepted 27th April 2020

DOI: 10.1039/d0cp01380c

rsc.li/pccp

## Introduction

Plants, algae and cyanobacteria harvest photons of visible light to convert solar light into chemical energy in a process known as oxygenic photosynthesis. The key reactions of this process are the extraction of electrons and protons from water and the reduction of carbon dioxide to carbohydrates. The final products, molecular oxygen and biomass, are essential for most life on Earth. Water oxidation to molecular oxygen is performed at the  $Mn_4Ca$  cluster of the oxygen-evolving complex (OEC) that resides within the transmembrane pigment–protein complex Photosystem II (PSII).<sup>1–5</sup> Driven by light-induced charge separations in the reaction center of PSII, the OEC cycles through five intermediate states,  $S_0$  through  $S_4$ , where the subscript indicates the number of oxidizing equivalents stored.<sup>6</sup> The  $S_4$  state is highly reactive and converts within milliseconds into the  $S_0$  state, releasing  $O_2$  and rebinding one ‘substrate water’ (the term is used independent of the protonation state).<sup>7</sup> If left

in the dark, the OEC will eventually relax into the dark-stable  $S_1$  state.<sup>8</sup>

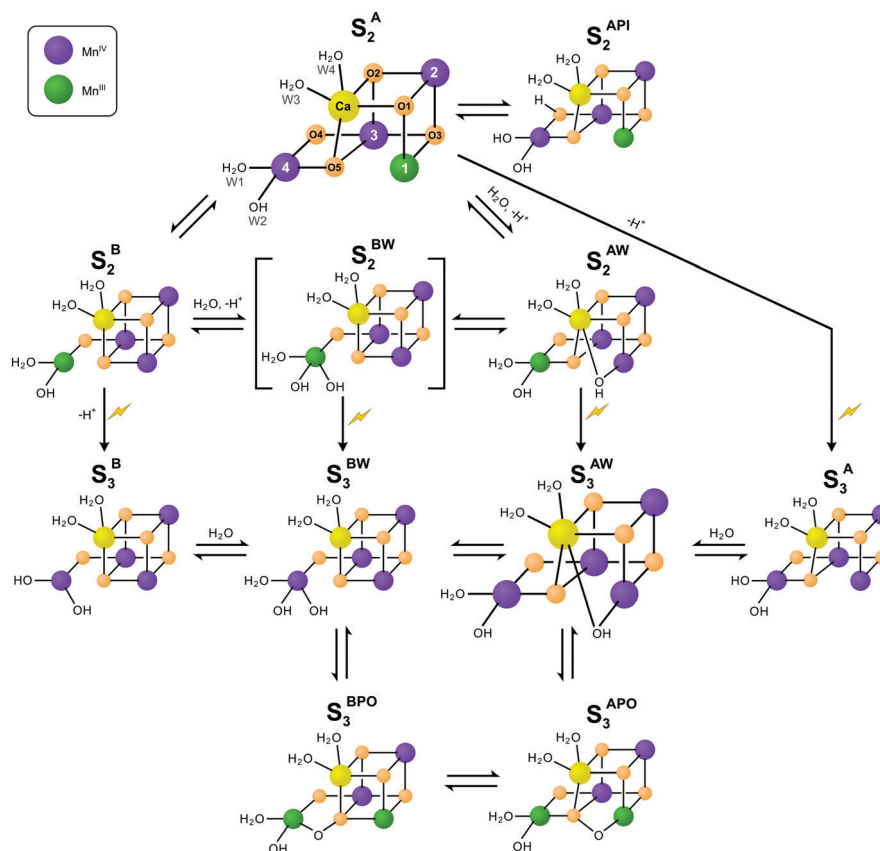
The lowest oxidation state of the  $Mn_4Ca$  cluster in the water splitting cycle, the  $S_0$  state, was shown by <sup>55</sup>Mn-ENDOR spectroscopy to have the oxidation states Mn(III,III,III,IV).<sup>9</sup> These overall ‘high’ oxidation states were recently confirmed by photoactivation experiments.<sup>10</sup> Each forward S-state transition involves the oxidation of one Mn(III) ion to Mn(IV) until Mn(IV,IV,IV,IV) is reached in the  $S_3$  state.<sup>3,11–19</sup> The  $S_3 \rightarrow S_4$  transition remains poorly understood and is suggested to lead to the formation of either an oxyl-radical, Mn(V,IV,IV,IV) or Mn(VII,III,III,III).<sup>11,20–22</sup>

The structure of the  $Mn_4Ca$  cluster was first reported at high resolution (1.9 Å and 1.95 Å) for the  $S_1$  state,<sup>23,24</sup> and recently also at resolutions between 2.0 Å and 2.1 Å for all S-states, except  $S_4$ .<sup>3</sup> (see also ref. 25). The  $S_0$ ,  $S_1$  and  $S_2$  states have similar structures, except that in  $S_0$  the Mn3–Mn4 distance is longer indicating that the O5 bridge is protonated.<sup>9,19,26</sup> This structure, often referred to as open cubane or A-type structure, is depicted schematically as  $S_2^A$  state in Scheme 1. The Ca ion and four Mn ions are connected by five oxo-bridges, and Ca and Mn4 bind two terminal water ligands each (W1–W4; W2 may be a hydroxo ligand).<sup>27–30</sup> The remaining coordination sites of the  $Mn_4Ca$  cluster are completed by bridging carboxy ligands

<sup>a</sup> Department of Chemistry, Umeå University, Linnaeus väg 6 (KBC huset), SE-901 87, Umeå, Sweden. E-mail: johannes.messinger@kemi.uu.se

<sup>b</sup> Molecular Biomimetics, Department of Chemistry – Ångström, Uppsala University, POB 523, SE-75120 Uppsala, Sweden





**Scheme 1** Isomers of the  $S_2$  and  $S_3$  states in photosystem II. The structures of the  $S_2^A$  and  $S_3^{AW}$  states were determined by X-ray crystallography; however, it remains controversial if the newly added oxygen bridge between Ca and Mn1 is an OH (as shown) or rather an oxo or oxyl.<sup>3,25</sup> Similarly, W2 may be a water instead of a hydroxide.<sup>27–30</sup> All other states are proposed on the basis of EPR spectroscopy and DFT calculations. Open cubane structures are labelled A, while closed cubane structures are signified with B. W indicates an additional hydroxo group, while PI signifies a proton isomer and PO the formation of a peroxidic intermediate.  $S_2^A$  has been assigned to the  $S_2^{LS}$  state, while there are three proposals for the  $S_2^{HS}$  state: the closed cube  $S_2^B$  state,<sup>40</sup> the hydroxo bound  $S_2^{AW}$  state<sup>41</sup> (see ref. 39 and 43 for related proposals), and the proton shift isomer  $S_2^{API}$ .<sup>42</sup> The  $S_2^{BW}$  state is shown in brackets since it is a proposed intermediate in the  $S_2 \rightarrow S_3$  transition<sup>55,98</sup> and for water exchange;<sup>81</sup> please note that the position of the Mn(III) valence and protonation states of oxygen ligands and bridges differ among the various suggestions. Evidence for the  $S_3^B$  or  $S_3^A$  states comes from EDNMR experiments indicating the presence of a five coordinate Mn(IV) ion under conditions preventing water binding.<sup>55</sup> The peroxide bound  $S_3$  states are consistent with early proposals by Renger,<sup>44</sup> and recent DFT calculations by the Yamaguchi group.<sup>57</sup> Labelling of atoms referred to in the text is provided in the  $S_2^A$  structure. Mn(IV) ions are shown in purple, Mn(III) in green, Ca in yellow and oxygen in orange. Transitions from one structure to the next may involve multiple steps.

supplied by the D1 and CP43 proteins of PSII (not shown). The only exception is the Mn1 site, which features one histidine ligand and is five-coordinate.<sup>3,11,31,32</sup>

While this  $S_2^A$  structure is the only one observed by crystallography, there is experimental and computational evidence for at least one additional conformation in the  $S_2$  state. The  $S_2$  state features two EPR signals at cryogenic temperatures: the low spin ( $S = 1/2$ )  $S_2$  EPR multiline signal ( $S_2^{LS}$ ) and the high-spin ( $S = 5/2$ )  $g = 4.1$  signal ( $S_2^{HS}$ ).<sup>33–35</sup> At near neutral pH values, the  $S_2^{LS}$  state is clearly dominant, and its structure is that of  $S_2^A$  (Scheme 1). The energy difference between the two  $S_2$  states and the transition state barrier between them are small enough so that the normally less stable  $S_2^{HS}$  state can be enriched in many ways, for example by illumination of  $S_1$  state samples at 130–140 K or by exposing the  $S_2^{LS}$  state to high pH (8.3–9.0), IR illumination or fluoride addition.<sup>34,36–38</sup> It is not clear if all  $S_2^{HS}$  states have the same structure, since slightly different  $g$  values in the range of 4.1–4.7 have been reported for the various conditions.<sup>39</sup> In

absence of a crystal structure for the  $S_2^{HS}$  state, the  $S_2^B$ ,  $S_2^{API}$  and  $S_2^{AW}$  structures have been proposed to give rise to the  $g = 4$  signal, where W indicates that an additional hydroxide is bound to the  $Mn_4Ca$  cluster, and PI signifies a proton isomer (Scheme 1).<sup>27–30,40–43</sup>

Among these, the closed cubane  $S_2^B$  state is the most prevalent suggestion for the  $S_2^{HS}$  state. The  $S_2^B$  state may be reached from the open cubane  $S_2^A$  state by moving the central O5 bridge away from Mn4 so that it instead forms a bond with Mn1. This structural change makes Mn4 five- and Mn1 six-coordinate, and is suggested to be accompanied by a valence swap between Mn4 and Mn1.<sup>30,40,45,46</sup> However, EXAFS experiments of samples in the  $S_2^{HS}$  state generated by 140 K illumination of  $S_1$  state samples result in Mn–Mn distances that are inconsistent with the  $S_2^B$  structure.<sup>47,48</sup> It was recently argued that the  $S_2^B$  state also does not provide a rational for many of the treatments leading to the  $S_2^{HS}$  state formation.<sup>42</sup> The latter study instead proposes a proton isomer of the  $S_2^A$  state as  $S_2^{HS}$  state ( $S_2^{API}$  in Scheme 1).



Since the high-pH induced  $S_2^{HS}$  state, in contrast to the  $S_2^{LS}$  state, can be advanced down to 77 K to the  $S_3^{AW}$  state, it was alternatively proposed that the  $S_2^{HS}$  state may already have the 'water' bound ( $S_2^{AW}$ ) that should otherwise insert during the  $S_2 \rightarrow S_3$  transition (see below).<sup>39,41,43</sup> It is noted that the Mn–Mn distances of the  $S_2^{AW}$  state are likely also not in line with the above discussed EXAFS data of the  $S_2^{HS}$  state generated by 140 K illumination.<sup>47</sup> The light-induced formation of the  $S_3$  state from  $S_2$  involves significant structural changes that include the binding of a water molecule in form of an additional oxo/hydroxo or oxyl bridge between Ca and Mn1 ( $S_3^{AW}$  in Scheme 1).<sup>3,11,13,25</sup> Even so, the precise molecular sequence for the formation of this sixth bridge remains controversial. Both the rotation of the Ca-bound W3 ligand towards Mn1, and the addition of W3 or a protein ligated water to Mn4 in combination with a pivot or carousel rearrangement of W1, W2 and O5 have been proposed.<sup>32,45,49,50</sup> Thus, starting from the  $S_2^A$  state, many different pathways can be envisioned for the formation of this most stable form of the  $S_3$  state ( $S_3^{AW}$  in Scheme 1). The structure of the  $S_3^{AW}$  state is well-characterized by X-ray crystallography and EPR spectroscopy.<sup>3,13,25</sup>

Importantly, EPR experiments additionally indicate the presence of an EPR-silent form of the  $S_3$  state that under IR illumination converts into the EPR-detectable  $S_2Y_Z^\bullet$  state.<sup>36,39,51</sup> This indicates that the  $Mn_4Ca$  cluster and D1-Tyr161 ( $Y_Z$ ), the electron donor to  $P680^{+}$ , are in a delicate redox equilibrium in the  $S_3$  state.<sup>52–54</sup> The EPR silent  $S_3$  state has been tentatively assigned to the  $S_3^B$  or  $S_3^{BW}$  structures.<sup>39</sup> Additionally, a recent EDNMR study of the  $S_3$  state identified a signal indicative of a five-coordinate Mn(IV) ion within the either the  $S_3^A$  or  $S_3^B$  structure.<sup>55</sup> Furthermore, peroxidic states ( $S_3^{APO}$ ,  $S_3^{BPO}$ ) have been proposed to exist in the  $S_3$  state.<sup>56–58</sup>

For determining the mechanism of O–O bond formation, which occurs during the  $S_3 \rightarrow S_4 \rightarrow S_0$  transition, it is crucial to identify the two substrate waters. Presently, the only technique able to probe the binding sites of substrate water in PSII is time-resolved membrane inlet mass spectrometry (TR-MIMS).<sup>7,59,60</sup> This method utilizes a rapid increase in  $H_2^{18}O$  concentration of the bulk water to determine the exchange rates of the two bound substrates by measuring the isotopic composition of  $O_2$  generated after various incubation times (Fig. 1).

TR-MIMS measurements show that the two substrate waters exchange with different rates. The slow exchanging substrate water ( $W_s$ ) is bound in all S-states. Its exchange rate slows 500-fold from  $S_0$  to  $S_1$ , increases 100-fold upon  $S_2$  formation and remains about the same in the  $S_3$  state despite the above described complexity of the  $S_2 \rightarrow S_3$  transition.<sup>7,60</sup> Importantly,  $W_s$  exchange is in all S states about 5–10 times faster in samples in which the natural Ca co-factor of the  $Mn_4Ca$  cluster is replaced by Sr (Sr-PSII).<sup>61</sup>

In the  $S_2$  and  $S_3$  states, TR-MIMS measurements can also resolve the exchange of the faster exchanging substrate water,  $W_f$ .<sup>62,63</sup> This shows that both substrates are bound to the OEC in the  $S_2$  state. Since protein- or Ca-ligated water molecules generally exchange at rates too fast for the present MIMS approach, this result indicates that  $W_f$  is Mn-bound in the

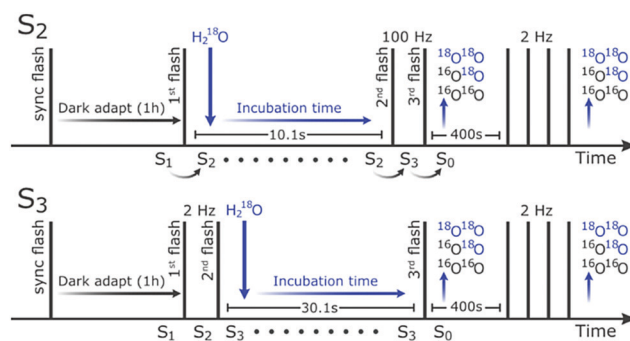


Fig. 1 Flash and injection scheme for TR-MIMS measurements in the  $S_2$ -state (top) and the  $S_3$ -state (bottom). Vertical lines indicate saturating flashes and the downward pointing arrows indicate injection of  $^{18}O$ -labelled water. The first flash was given to synchronize the samples in the  $S_1Y_D^0$  state, while the final group of four flashes is employed for normalization.

$S_2$  state and that the new water molecule binding in the  $S_2 \rightarrow S_3$  transition is not a substrate in the ongoing S-state cycle. Consequently, we suggested  $W_2$  as candidate for  $W_f$ .<sup>7,60,64</sup> As noted in these studies, this conclusion does not hold if the exchange of  $W_f$  is limited by the diffusion of water through the protein channels.

Together with structural information available at the time,<sup>26,65</sup> the TR-MIMS data led to the proposal that the central oxygen bridge between Ca and two Mn ions, now referred to as  $O_5$ , is the slow exchanging substrate  $W_s$  that forms the O–O bond with  $W_2$  in a  $S_2^B$  like conformation.<sup>64</sup> A related, more detailed proposal for the mechanism of water oxidation that involves a similar O–O bond formation mechanism, but utilizes a  $S_3^{AW}$  like conformation, was later made on the basis of DFT calculations.<sup>66</sup> Importantly, subsequent advanced EPR measurements have demonstrated that  $O_5$  exchanges fast enough with bulk water to be compatible with  $W_s$  exchange kinetics observed by TR-MIMS.<sup>67</sup> Nevertheless,  $W_2$ ,  $W_3$  and  $O_4$  have been suggested by other groups to be the slow substrate water instead of  $O_5$ .<sup>68–70</sup>

Up to now, all TR-MIMS measurements were performed under conditions where the open cubane states are predominant. To compare the substrate water exchange rates in the two structural forms of the  $S_2$  state, we followed in this study a recently developed protocol for enriching PSII core preparations from *Thermosynechococcus elongatus* (*T. elongatus*) in either the  $S_2^{LS}$  or the  $S_2^{HS}$  state.<sup>38</sup> The data presented below provide unique insights into the pathway of substrate water exchange and the binding sites of  $W_f$  and  $W_s$ .

## Experimental procedure

### Photosystem II core preparation

The *T. elongatus*  $\Delta psbA1 \Delta psbA2$  deletion mutant<sup>71,72</sup> was grown in Ca- or Sr-containing buffers, and the PSII core preparations were isolated and purified as described previously.<sup>73,74</sup> After preparation, the PSII cores were washed with an aqueous solution of 1 M betaine, 15 mM  $CaCl_2$  and 15 mM  $MgCl_2$ , in an Amicon Ultra-15 centrifugal filter unit (cut-off 100 kDa) until





the estimated residual MES concentration was smaller than 1  $\mu\text{M}$ . Finally, the samples were frozen in liquid nitrogen until used.

### Time-resolved membrane inlet mass spectrometry

For TR-MIMS measurements, an isotope ratio mass spectrometer (Finnigan Delta plus XP) was used. The spectrometer was connected to a membrane inlet rapid mixing cell (volume of 165  $\mu\text{l}$ ) via a steel pipe that runs through a cooling trap containing ethanol/dry ice.<sup>59,62</sup>

For each measurement, an aliquot of PSII cores was thawed on ice and then diluted 10-fold into an unbuffered solution containing 15 mM  $\text{CaCl}_2$ , 15 mM  $\text{MgCl}_2$  and 1 M Betaine. To fully oxidize tyrosine D, the samples were then exposed to a saturating xenon-flash (full width at half maximum  $\approx 5 \mu\text{s}$ ), followed by 60 min dark adaptation at 20  $^\circ\text{C}$ , during which the sample was loaded into the MIMS chamber. Five minutes before the measurements, the pH was adjusted by injecting 8  $\mu\text{l}$  of 1 M buffer (see below) containing 2 mM of the artificial electron acceptor 2,6-dimethyl-1,4-benzoquinone (DMBQ), from a 50 mM stock solution in dimethyl sulfoxide. The final concentrations were 0.29 mg of Chl  $\text{ml}^{-1}$ , in 50 mM buffer (MES pH 6.0, TAPS pH 8.3 for Sr-PSII or TAPS pH 8.6 for Ca-PSII) and 100  $\mu\text{M}$  DMBQ. The slightly lower pH used for Sr-PSII was chosen to ensure the integrity of the Sr-PSII samples. We note that the  $\text{S}_2^{\text{LS}}$  to  $\text{S}_2^{\text{HS}}$  conversion was nearly complete at this pH for Sr-PSII, while pH 8.6 was required to achieve a similar conversion in Ca-PSII.<sup>38</sup> For measurements with ammonia, a final concentration of 50 mM  $\text{NH}_4\text{Cl}$  was employed.

Rapid enrichment of the sample with  $\text{H}_2^{18}\text{O}$  was achieved by means of a modified gas-tight syringe (Hamilton CR-700-200) that was driven by air-pressure via a fast-switching solenoid valve ( $k_{\text{inj}} = 170 \text{ s}^{-1}$  based on fluorescence rise after injections of fluorescein; see also ref. 59, 63 and 75). To minimize artifacts from dissolved oxygen, the syringe was loaded with 97%  $\text{H}_2^{18}\text{O}$  in a  $\text{N}_2$ -filled glove box. The  $\text{H}_2^{18}\text{O}$  was further deoxygenated with a mixture of glucose/glucose oxidase (Sigma Aldrich, *A. niger*) and catalase (Sigma Aldrich, *B. taurus*).<sup>59</sup>

The measurement consisted of a series of saturating flashes and a single injection as shown in Fig. 1. After synchronization in the  $\text{S}_1\text{Y}_D^{\text{ox}}$  state, the PSII samples were illuminated with one ( $\text{S}_2$ ) or two (2 Hz;  $\text{S}_3$ ) saturating flash(es) to advance the majority of the centers from the  $\text{S}_1$  state to the desired S-state. This step was followed by a fixed delay (10.1 s for the  $\text{S}_2$  and 30.1 s for the  $\text{S}_3$  state) before the  $\text{O}_2$ -generating flash(es) were given (two at 100 Hz for  $\text{S}_2$ , and one in case of  $\text{S}_3$ ) that advanced the enzyme via the  $\text{S}_4$  state to the  $\text{S}_0$  state. At various times  $t_i$  before the  $\text{O}_2$ -generating flash(es), the  $\text{H}_2^{18}\text{O}$  was injected into the PSII sample resulting in the reported incubation times. After a delay of 400 s, which allowed all signals to return to baseline levels, the PSII samples were exposed to four more flashes given at 2 Hz. This signal was used for normalization, and for determining the relative flash-induced oxygen evolution activity, which was, at pH 8.6, 50% of that at pH 6.0, independent of the ammonia addition.

The mass-to-charge ratios  $m/z$  34 and  $m/z$  36 were monitored for determination of the flash-induced  $\text{O}_2$ -production in PSII,

while  $m/z$  40 (Ar) was recorded as a reference. The  $\text{H}_2^{18}\text{O}$  enrichment after complete mixing was calculated from the  $m/z$  34/36 ratio of the four normalizing flashes to be  $\approx 20\%$ .<sup>59,62</sup> Data points recorded at short incubation times that approached the mixing time were corrected for the change in isotopic enrichment and PSII concentration as described previously.<sup>59,62,75</sup>

### Kinetic modelling of substrate exchange

Exchange rates ( $k_f$ ,  $k_i$ ,  $k_s$ ) were determined by simultaneous fitting of the corrected  $^{16,18}\text{O}_2$  and  $^{18,18}\text{O}_2$  data to eqn (1) and (2).<sup>59,62</sup> The pre-exponential  $a$  represents the ratio between fast and slow exchange in the  $^{16,18}\text{O}_2$  data. It was calculated from the initial  $\text{H}_2^{18}\text{O}$  enrichment ( $\alpha_{\text{in}}$ ; 0.07%), which was determined slightly higher than natural abundance due to a small leakage from the syringe tip, and the final ( $\alpha_f$ )  $\text{H}_2^{18}\text{O}$  enrichment using eqn (3). The pre-exponential  $b$  represents the ratio between two distinct populations of slowly exchanging substrate waters.  $b$  was determined from an initial separate fit of the normalized  $^{36}\text{O}_2$  yield to eqn (2). Both parameters,  $a$  and  $b$ , were held constant in the final global fit of the  $m/z$  34 and 36 data.

$$\frac{m}{z}34 = a \cdot (1 - e^{-k_f \cdot t}) + (1 - a)(b \cdot (1 - e^{-k_i \cdot t}) + (1 - b) \cdot (1 - e^{-k_s \cdot t})) \quad (1)$$

$$\frac{m}{z}36 = b \cdot (1 - e^{-k_i \cdot t}) + (1 - b) \cdot (1 - e^{-k_s \cdot t}) \quad (2)$$

$$a = \frac{\alpha_f \cdot (1 - \alpha_{\text{in}}) + (1 - \alpha_f) \cdot \alpha_{\text{in}}}{(1 - \alpha_f) \cdot \alpha_f \cdot 2} \quad (3)$$

Activation energies were calculated according to the transition state theory:

$$E_A = RT \left( \ln \left( \frac{k_B T}{h} \right) - \ln(k) \right) \quad (4)$$

where  $R$  is the gas constant,  $T$  the temperature ( $T = 293 \text{ K}$ ),  $k_B$  the Boltzmann constant and  $k$  the rate of the reaction. The exchange pathways I and II (Fig. 4) were modelled and compared to the best fits using an Excel spread sheet.

## Results

Fig. 2 shows the results of the substrate water exchange experiments in the  $\text{S}_2$  state of PSII core samples from *T. elongatus* containing the natural Ca cofactor in the OEC (Ca-PSII) or instead Sr (Sr-PSII). Each dot represents the normalized flash-induced yield of dioxygen produced after the exchange of one ( $^{16,18}\text{O}_2$ ;  $m/z$  34) or both ( $^{18,18}\text{O}_2$ ;  $m/z$  36) substrate waters during a discrete time of incubation with  $\text{H}_2^{18}\text{O}$  enriched water. For Ca-PSII at pH 6.0, the typical biphasic rise of the  $m/z$  34 signal was observed (Fig. 2A, black points). The biphasic nature of this signal reflects the independent exchange of the two substrate waters,  $W_f$  and  $W_s$ , with bulk water at rates  $k_f$  and  $k_s$ .<sup>7,59,62</sup> The corresponding rise of the  $^{18,18}\text{O}_2$  signal at  $m/z$  36 (Fig. 2B, black dots), which requires the exchange of both substrate water molecules, shows the previously reported monophasic rise with



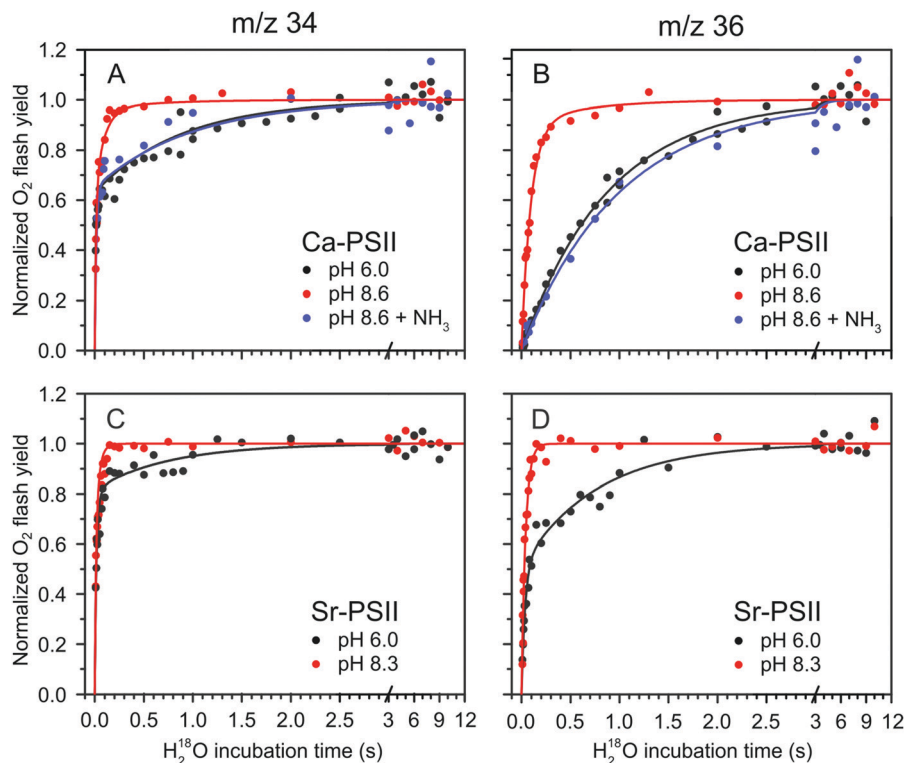


Fig. 2  $\text{H}_2^{18}\text{O}$  substrate exchange of Ca-PSII (A) and (B) and Sr-PSII (C) and (D) in the  $\text{S}_2$ -state. (A) and (C) represent the normalized flash yields of single-labelled dioxygen ( $m/z$  34), while (B) and (D) represent the normalized flash yields of double-labelled dioxygen ( $m/z$  36). Black dots represent measurements performed at pH 6.0, while red dots are data from measurements taken at pH 8.6 for Ca-PSII and at pH 8.3 for Sr-PSII. Blue dots signify the results of experiments with Ca-PSII at pH 8.6 in presence of 50 mM  $\text{NH}_4\text{Cl}$ . Lines are fits according to eqn (1)–(3), of which the parameters are given in Table 1.

rate  $k_s$ , corresponding to the slow component of the  $m/z$  34 rise in Fig. 2A. These results are consistent with a single conformation ( $\text{S}_2^{\text{LS}} = \text{S}_2^{\text{A}}$ ) for the  $\text{S}_2$  state under these conditions, which is in line with EPR spectroscopy performed previously under the same conditions on the same type of samples.<sup>38</sup> The data were thus fit employing eqn (1) and (2), using only two kinetic components ( $b$  was set to zero).<sup>59,62</sup> The parameter of the best fits (solid lines in Fig. 2A and B) are given in Table 1. The results are fully consistent with previous measurements.<sup>63,76,77</sup>

The TR-MIMS data for Sr-PSII at pH 6.0 are displayed in Fig. 2C and D (black points). It is clearly seen in Fig. 2D that the rise of the

$m/z$  36 signal was biphasic, with the two phases having comparable amplitudes: a slow phase with a rate  $k_s$  similar to that seen in Ca-PSII, and a 20–30 times faster phase, designated here as the intermediate phase, with rate  $k_i$  (eqn (2) and Table 1). Such a biphasic behavior of the  $m/z$  36 data was not reported previously. It can best be rationalized by the presence of two distinct forms of the  $\text{S}_2$  state in Sr-PSII that are in slow equilibrium at room temperature. The proposed presence of two conformations in Sr-PSII is in agreement with recent low temperature EPR data showing that the  $\text{S}_2^{\text{LS}}$  and  $\text{S}_2^{\text{HS}}$  EPR signals coexist under these conditions (yet  $\text{S}_2^{\text{HS}}$  being present at lower ratio).<sup>38</sup>

**Table 1** Summary of parameters extracted from the global fits of the mass-to-charge ratio signals  $m/z$  34 ( $^{16,18}\text{O}_2$ ) and  $m/z$  36 ( $^{18,18}\text{O}_2$ ) displayed in Fig. 2 by employing eqn (1)–(3). The  $\text{H}_2^{18}\text{O}$  substrate exchange measurements of Ca-PSII and Sr-PSII core preparations from *T. elongatus* in the  $\text{S}_2$  and  $\text{S}_3$  states were performed at 20 °C and the indicated conditions ( $\text{NH}_3$  signifies addition of 50 mM  $\text{NH}_4\text{Cl}$ ). The rate  $k_f$  describes the fast exchange phase with the amplitude  $a$  in  $m/z$  34, which is assigned to the fast exchanging water ( $W_f$ ), while  $k_i$  describes the intermediate phase, which is resolved in some of the  $m/z$  36 data with the amplitude  $b$ . The parameter  $k_s$  describes the slowest exchange rate resolved in the  $m/z$  36 data with the amplitude  $1 - b$ . The rate constants  $k_i$  and  $k_s$  are both assigned to the slow exchanging water  $W_s$ . The amplitude  $a$  varies due to small differences in the final  $\text{H}_2^{18}\text{O}$  enrichment

Sample		S state	Conditions	$W_{\text{f}} k_{\text{f}} \text{ (s}^{-1}\text{)}$	$W_{\text{s}} k_{\text{i}} \text{ (s}^{-1}\text{)}$	$W_{\text{s}} k_{\text{s}} \text{ (s}^{-1}\text{)}$	$a$	$b$
Ca-PSII	This study	S <sub>2</sub>	pH 6.0	102 ± 9	—	1.14 ± 0.03	0.63	0
	This study	S <sub>2</sub>	pH 8.6	75 ± 7	10.5 ± 0.6	1.6 ± 0.9	0.63	0.9
	This study	S <sub>2</sub>	pH 8.6 + NH <sub>3</sub>	64 ± 18	—	1.02 ± 0.09	0.65	0
	Ref. 77	S <sub>3</sub>	pH 6.5	40 ± 4	—	0.69 ± 0.06	0.65	0
	This study	S <sub>3</sub>	pH 8.6	19.5 ± 2.2	—	0.25 ± 0.01	0.65	0
Sr-PSII	This study	S <sub>2</sub>	pH 6.0	85 ± 10	29.7 ± 3.2	1.5 ± 0.1	0.63	0.49
	This study	S <sub>2</sub>	pH 8.3	76 ± 7	24.3 ± 1.1	—	0.65	1.0



Given the observation of two rates for  $W_s$  exchange, the  $m/z$  34 rise was fit with three kinetic components according to eqn (1). The resulting  $W_f$  exchange rate for the  $S_2$  state was found to be similar to that measured in Ca-PSII at the same pH value.

At pH 8.6/pH 8.3, a strong acceleration in the exchange rate of the slow substrate was observed for both Ca-PSII and Sr-PSII samples (red dots and lines in Fig. 2). This rate was similar to  $k_i$  observed at pH 6.0 in Sr-PSII, and accounted for 90% of the rise of the  $m/z$  36 signal in the Ca-PSII samples, and for 100% in case of the Sr-PSII samples. This is fully consistent with the near total conversion of the multiline signal into the  $g = 4$  signal observed by EPR under these conditions.<sup>38</sup> Table 1 shows that the rate constants  $k_f$  and  $k_s$  are essentially insensitive to pH and Ca/Sr substitution. In Sr-PSII,  $k_i$  is also essentially unaffected by pH, but the  $k_i$  of Sr-PSII is larger by a factor of 2–3 compared to that of Ca-PSII.

It was recently demonstrated that addition of ammonia to PSII core complexes from *T. elongatus* in a pH 8.6 buffer leads to the quasi quantitative formation of the ammonia modified  $S_2$  multiline signal ( $S_2^{LS}$ ) at the expense of the  $g = 4$  signal ( $S_2^{HS}$ ).<sup>38</sup> Employing this treatment we tested whether the accelerated water exchange is caused by the high pH or instead is related to the different structures of the  $Mn_4Ca$  cluster in the  $S_2^{LS}$  and  $S_2^{HS}$  states (blue dots and lines in top panels of Fig. 2). It can be seen that ammonia addition essentially reverted the rates to those seen at pH 6.0 (black data points). This strongly suggests that the water exchange rates observed are a direct consequence of the conformation of the  $Mn_4Ca$  cluster, rather than pH. In agreement with this conclusion, ammonia had very little effect on the substrate exchange kinetics at lower pH, where basically only the  $S_2^A$  state was present in Ca-PSII samples.<sup>76</sup>

In contrast to the slowly exchanging substrate water  $W_s$ , only minor variations were observed for the exchange rate of the fast exchanging substrate  $W_f$  in the  $S_2$  state under all conditions (Fig. 2A, C and Table 1). The lack of any significant effect of the substitution of Ca by Sr in the  $S_2$  state is especially notable, and indicates that W3 is either not a substrate (that possibly binds

as Ox/O6 in the  $S_3$  state), or its exchange at the Ca site is limited by factors other than breaking the bond to Ca/Sr, such as for example the diffusion of bulk water through water channels.

Fig. 3 shows the substrate water exchange in the  $S_3$  state in Ca-PSII core complexes of *T. elongatus* at pH 8.6. These experiments revealed that the rate of  $W_s$  exchange in the  $S_3$  state is well described by a monophasic rise (red dots and line in Fig. 3). In stark contrast to  $S_2$ ,  $k_s$  was in the  $S_3$  state slower at pH 8.6 than observed previously at neutral pH (dashed black line in Fig. 3).<sup>55,78</sup> This results in a 6-fold difference between the slow substrate water exchange rates of the  $S_2$  and  $S_3$  states at pH 8.6 (Table 1), indicating that the substrate exchange in the  $S_2$  and  $S_3$  states is governed by different exchange mechanisms and rate limiting steps. Thus, the previously found near identical exchange rate for these two S-states appears to be coincidental.

### Mechanistic and energetic analysis

The fact that two different rates of  $W_s$  exchange were measured under the same conditions (Fig. 2C) implies that the equilibrium between the two  $S_2$  state conformations has a similar or higher barrier than substrate water exchange. Thus, two possibilities exist: (I) there are two independent exchange pathways for  $W_s$  in the  $S_2^{LS}$  and  $S_2^{HS}$  states, of which the  $S_2^{HS}$  exchange has a lower barrier (exchange pathway I in Fig. 4), or (II) the  $S_2^{LS}$  conformation has to convert into the  $S_2^{HS}$  conformation so that water exchange can occur (pathway II in Fig. 4). In these two schemes, the rate  $k_s$  corresponds to the exchange of  $W_s$  that starts from the  $S_2^{LS}$  conformation; it thus reports either on the activation energy for the exchange process starting from this structure (pathway I), or on the energetic barrier for reaching the  $S_2^{HS}$  conformation (pathway II). Since  $k_s$  is nearly pH and Ca/Sr independent (Table 1), it must be the energy difference between the  $S_2^{LS}$  and  $S_2^{HS}$  conformations that changes at high pH. Furthermore, as the HS state is stabilized at high pH, it is likely that a deprotonation is involved in the  $S_2^{LS} \rightarrow S_2^{HS}$  conversion, as suggested previously.<sup>38</sup> By contrast, the rate  $k_i$  signifies in both pathways the  $W_s$  exchange rate starting from the  $S_2^{HS}$  conformation.

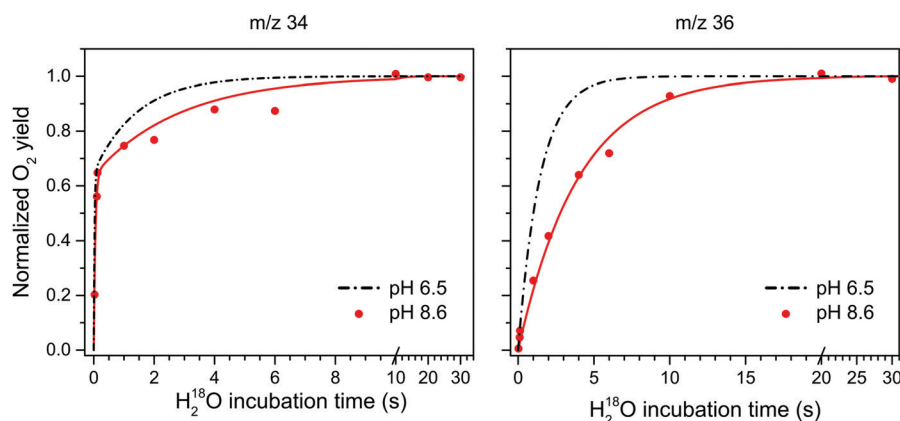


Fig. 3  $H_2^{18}O$  substrate exchange of Ca-PSII at pH 8.6 in the  $S_3$  state. Red dots represent the results from single time points. Red lines are fits according to eqn (1)–(3), while the black dashed lines represent simulated exchange rates based on literature values of exchange in similar preps and conditions, but at pH 6.5.<sup>77</sup> The fitted exchange rates are listed in Table 1.



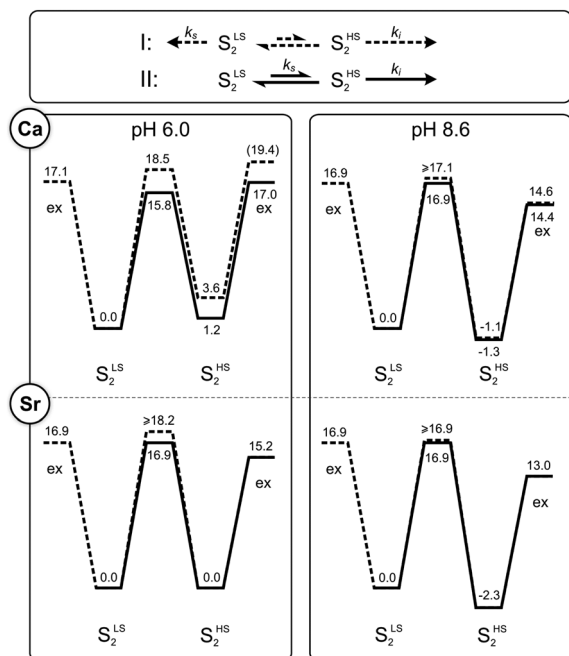


Fig. 4 Kinetic models (top panel) and energy diagrams (lower panels) for the exchange ('ex') of the slow substrate water  $W_s$  in the  $S_2^{LS}$  and  $S_2^{HS}$  conformations of photosystem II. The barriers were calculated from the rates listed in Table 1 using transition state theory (eqn (4)). They are given in kcal mol<sup>-1</sup>. Dashed lines correspond to pathway I, where  $S_2^{LS}$  and  $S_2^{HS}$  exchange independently, while solid lines represent the sequential pathway II, in which the  $S_2^{LS}$  conformation has to convert first into the  $S_2^{HS}$  conformation before water exchange can occur. Where lines overlap, only the solid line is visible. The length of the arrows in the top panel correspond to the rates of  $W_s$  exchange in Ca-PSII at pH 6.0.

This rate is also nearly pH independent, but  $k_i$  is about three-fold larger in Sr-PSII than in Ca-PSII.

Employing the Eyring equation (eqn (4)), energy diagrams for the two exchange pathways were established for Ca- and Sr-PSII at both pH regimes (Fig. 4). The energy diagrams shown are not unique in all aspects, but rather the simplest ones we could conceive to explain our findings with minimal variations of parameters. As such, the relative energy levels of  $S_2^{LS}$  and  $S_2^{HS}$  were adjusted to reflect the percentages of centers undergoing intermediate and slow water exchange as reflected in the  $m/z = 36$  data.

In the sequential exchange pathway II, shown in black lines in Fig. 4, the energy of the  $S_2^{HS}$  conformation is by 1.2 kcal mol<sup>-1</sup> higher than that of the  $S_2^{LS}$  conformation in Ca-PSII at pH 6. This value is highly similar to that determined by previous DFT calculations that were based on the proposal that the  $S_2^{HS}$  conformation attains the  $S_2^B$  structure.<sup>40,45</sup> Substitution of Ca by Sr makes the two conformations of the  $S_2$  state iso-energetic at pH 6, while the increase of pH to 8.3/8.6 stabilizes the  $S_2^{HS}$  state by 2.3–2.5 kcal mol<sup>-1</sup> in both samples. Within the sequential exchange pathway,  $k_s$  is a direct measure of the activation energy of the  $S_2^{LS} \rightarrow S_2^{HS}$  transition. A value of 15.8 kcal mol<sup>-1</sup> was found for Ca-PSII at pH 6, while it was 16.9 kcal mol<sup>-1</sup> under all other conditions tested here. This is higher than estimated in two previous DFT studies that modeled the HS to LS conversion to be a shift of O5 between Mn4 and Mn1

(6–11 kcal mol<sup>-1</sup> for Ca and Sr).<sup>40,45,79</sup> It is also more than twice the value (6.5 kcal mol<sup>-1</sup>) derived in one EPR study that followed the rate of  $S_2^{HS}$  to  $S_2^{LS}$  conversion in a temperature range between 150–170 K (see also ref. 100).<sup>80</sup> However, the value is rather similar to the barrier (17.6 kcal mol<sup>-1</sup>) calculated by Siegbahn for the exchange of O5 in the  $S_2$  state.<sup>81</sup>

Similar energy levels and barriers were obtained when examining the alternative parallel exchange pathway I (dashed lines in Fig. 4). The main difference is that the barrier between  $S_2^{LS}$  and  $S_2^{HS}$  must be higher to block water exchange of centers in the  $S_2^{LS}$  state via the  $S_2^{HS}$  route.

## Discussion

In this study, we examined the exchange rates of the two substrate water molecules in the  $S_2^{LS}$  and  $S_2^{HS}$  conformations of PSII-core preparations of *T. elongatus* by pH shifts, ammonia addition and Ca/Sr substitution. We report for the first time that the slowly exchanging substrate water,  $W_s$ , equilibrates 10 times faster in the  $S_2^{HS}$  state than in the  $S_2^{LS}$  ( $S_2^A$ ) state. While we employed a pH shift for switching between the two conformations of the  $S_2$  state,<sup>38</sup> we excluded that the observed changes in rates are a consequence of the different proton concentrations by adding ammonia, which was previously shown to stabilize the  $S_2^{LS}$  configuration at high pH by directly binding to Mn.<sup>38,76,82–84</sup> We also discovered that at alkaline pH the slow substrate water no longer exchanges with similar rate in the  $S_2$  and  $S_3$  states, and that the exchange rate of the fast exchanging substrate water is not only insensitive to Ca/Sr substitution in the  $S_3$  state, as reported previously, but also in the  $S_2$  state.

Below we discuss these three new findings in detail on the basis of present structural knowledge about the Mn<sub>4</sub>Ca cluster and with regard to the only detailed exchange pathway that has been proposed thus far for O5. The aim of the discussion is to both gain an improved understanding of the mechanism of substrate water exchange, and to scrutinize the presently favored assignments of  $W_s$  to O5 and of  $W_f$  and  $W_2$  or  $W_3$ . This task is complicated by the fact that there is an ongoing vivid discussion regarding the structure of the  $S_2^{HS}$  state, with no less than 3 different proposals. This uncertainty in the field necessitates to discuss a variety of options. After identifying the assignments for the substrates consistent with our present and previous data, we formulate consequences for current proposals for the mechanism of water oxidation in PSII.<sup>7,11,63,64,85–87</sup>

## General considerations

Water exchange can follow an associative or dissociative pathway. In the former, a new water molecule binds first before the original water molecule is released into the bulk, while in the latter, the coordinated water molecule dissociates before a new water can bind. Ligand exchange rates are known to slow down with increasing metal oxidation state, and Mn(IV) is generally seen as being exchange inert, while in case of Mn(III) at least the water bound along the Jahn–Teller (JT) axis should be readily





exchangeable.<sup>60,81,88–94</sup> If water is bound in a deprotonated form, it needs to be protonated, and bridging oxygen's need additionally be brought into a terminal position before exchange with bulk water can occur. This implies that the exchange of O5 is a complex process that requires conformational changes of the Mn<sub>4</sub>Ca cluster, likely involving a number of the proposed structures summarized in Scheme 1.

### Evaluation of O5 as the slowly exchanging substrate water $W_s$

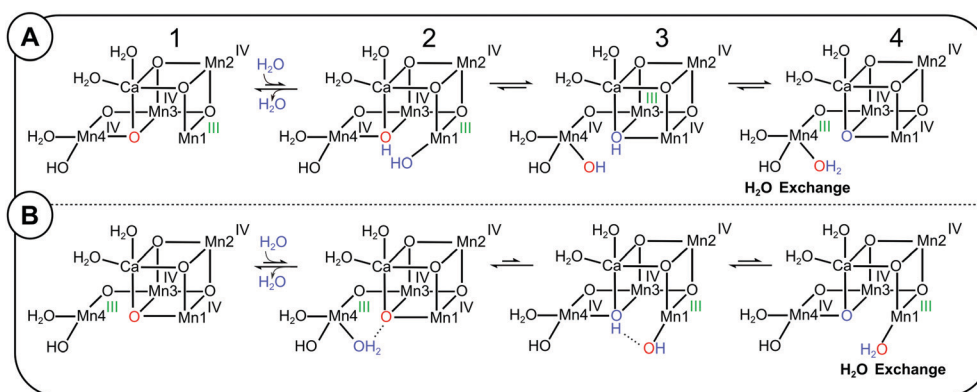
On the basis of substrate water exchange experiments<sup>64</sup> and theoretical calculations,<sup>11</sup> it was postulated that O5 is the slowly exchanging substrate  $W_s$ . The rationale for the experimental assignment was twofold: firstly, the exchange rate of  $W_s$  is dependent on both Ca/Sr substitution and S-state; thus  $W_s$  was suggested to be a bridge between Mn and Ca.<sup>61,64</sup> Secondly, this bridge was assigned to O5,<sup>64</sup> because EPR and EXAFS data are indicative of its deprotonation during the  $S_0 \rightarrow S_1$  transition,<sup>9,11,18,19,26,27</sup> matching the 500-fold decrease in substrate exchange rate between  $S_0$  and  $S_1$ .<sup>95</sup> Subsequent EDNMR experiments have confirmed that O5 exchanges with bulk water within 15 s in the  $S_1$  state,<sup>67</sup> which is unusually fast for a  $\mu$ -oxo bridge,<sup>92</sup> and this finding makes O5 a candidate for  $W_s$ . However, a definitive assignment needs to await a higher time resolution that allows matching the EDNMR-based O5 exchange kinetics with those obtained for  $W_s$  by TR-MIMS.

In 2013, Siegbahn proposed a mechanism for the exchange of O5 with bulk water.<sup>81</sup> Starting from the  $S_2^A$  conformation (2A-1), the first step is the binding of a bulk water molecule (marked blue in Scheme 2A) to the open coordination site of Mn1. This step, which has a calculated barrier of 17.6 kcal mol<sup>−1</sup> and is thus rate limiting for the O5 exchange,<sup>81</sup> results in a structure (2A-2) resembling  $S_2^{AW}$ , but with one additional proton on O5 and swapped oxidation states. Next, the newly inserted hydroxo swings into the O5 binding site and O5H becomes a terminal ligand of Mn4 (2A-3). The new bridging OH transfers its

proton to form a fully protonated terminal O5 ligand on Mn4(IV). After a valence swap between Mn4 and Mn3 the Mn4(III)–O5H<sub>2</sub> conformation is reached (2A-4; a  $S_2^{BW}$  like structure with one additional proton) that allows O5 to exchange with bulk water, presumably *via* a dissociative mechanism. Thereafter, this multi-step sequence reverses to yield back the  $S_2^A$  state, but with O5 exchanged from <sup>16</sup>O to <sup>18</sup>O.

It is important to note that the  $S_2^{BW}$  conformation reached *via* this Mn4-site exchange pathway is fundamentally different from the  $S_2^B$  conformation formed *via* the  $S_2^A \leftrightarrow S_2^B$  equilibrium proposed by the Pantazis, Guidoni and Yamaguchi groups.<sup>32,40,96,97</sup> The important difference is that the original O5 (red) is bound terminally to Mn4(III), and not as a  $\mu$ -3-oxo between Ca, Mn3 and Mn1 (Scheme 1). Therefore, the  $S_2^B$  conformation is not an intermediate of Siegbahn's Mn4-site exchange mechanism of O5.

Thus, if the frequently accepted proposals that, firstly,  $S_2^B$  is the structure of the  $S_2^{HS}$  conformation and, secondly, the Mn4-site exchange mechanism describes the exchange of  $W_s$  are both correct, then it follows that the 10-fold faster exchange of  $W_s$  in the  $S_2^{HS}$  conformation cannot be understood within a sequential exchange mechanism in which  $S_2^A$  converts first into  $S_2^B$  before water exchange can take place (pathway II in Fig. 4). Accordingly, a separate pathway starting from the  $S_2^{HS}$  state must be considered that can explain the 10-fold faster  $W_s$  exchange in this conformation (Scheme 2B; Mn1-site O5 exchange pathway). The first step is water binding to Mn4, which induces a flip of bonds and charges akin to the pivot and carousel mechanisms describing water binding during the  $S_2 \rightarrow S_3$  transition (2B-1 to 2B-4).<sup>7,32,49,98</sup> This is essentially the reverse of the Mn4-site exchange pathway (Scheme 2A), and places O5 in a  $S_2^{AW}$  like structure into a terminal position at Mn1(III), where it may exchange with bulk water, possible *via* Ca. However, since it is not obvious why this pathway would have a lower barrier than the Mn4 exchange pathway, we presently disfavor this option.



**Scheme 2** Possible exchange pathways for O5 starting from the  $S_2^S$  state (panel A) and the  $S_2^{HS}$  state (panel B). (A) Mn4 site O5 exchange mechanism (redrawn after ref. 81). A bulk water or  $W_3$  (blue) binds to Mn1 in the  $S_2^A$  conformation, leading to a valence flip between Mn4 and Mn3, and the transfer of one proton from the new water to O5 (red). The final conformation has a water-bound  $S_2^B$ -type structure, in which Mn4 has the oxidation state III (green), allowing the exchange of O5 before returning to the  $S_2^A$  conformation by reversing the sequence. (B) Proposal of a Mn1-site O5 exchange pathway starting from the  $S_2^B$  conformation. A water (blue) binds to the five coordinated Mn4(III) in the  $S_2^B$  conformation, which induces a proton transfer and valence flip that leads to the formation of a water-bound  $S_2^A$  conformation, in which O5 is bound to the five-coordinated Mn1(III) site, where water exchange may occur.



Looking at the two other structural proposals for the  $S_2^{\text{HS}}$  state (Scheme 1), it is noted that the  $S_2^{\text{AW}}$  conformation may provide an explanation for the faster exchange of O5 in the  $S_2^{\text{HS}}$  state, since it resembles the first intermediate of the Mn4 exchange pathway (2A-2; note the different oxidation state assignments and the extra proton). Indeed, the energy barrier determined here for the  $S_2^{\text{LS}} \rightarrow S_2^{\text{HS}}$  conversion is with 16 to 17 kcal mol<sup>-1</sup> similar to that calculated by Siegbahn for the first step of the Mn4-site exchange pathway for O5 (17.6 kcal mol<sup>-1</sup>).<sup>81</sup> Similar values for water binding to Mn1 (in the  $S_2 \rightarrow S_3$  transition) were obtained by Guidoni and Pantazis.<sup>32,99</sup> By contrast, the theoretical estimates for  $S_2^{\text{A}} \rightarrow S_2^{\text{B}}$  (6–11 kcal mol<sup>-1</sup>) are significantly lower,<sup>40,45,46</sup> as are previous experimental determinations of the barrier for the  $S_2^{\text{HS}}$  to  $S_2^{\text{LS}}$  conversion that gave values of  $6.7 \pm 0.5$  kcal mol<sup>-1</sup> and  $7.9 \pm 1.4$  kcal mol<sup>-1</sup>, respectively.<sup>80,100</sup> These previous experimental barriers were obtained by generating the  $S_2^{\text{HS}}$  state from  $S_1$  by illumination at 130–135 K in spinach PSII membrane fragments, and measuring the temperature dependence of the conversion of the  $g = 4.1$  signal into the  $S_2$  multiline signal in the temperature range of 150–170 K. Thus, the experimental conditions are highly different from the ones in the present study, where for the first time this barrier was determined at physiological temperatures that facilitate protonation state and structural changes, including water binding. By contrast, such changes are inhibited in *T. elongatus* PSII samples at cryogenic temperatures, as indicated by the experiments by Boussac, in which he needed to warm the samples to room temperature for a few seconds to allow the conversion of the  $S_2^{\text{LS}}$  state into the  $S_2^{\text{HS}}$  state after a 200 K illumination at alkaline pH.<sup>38</sup> As such it seems likely that the  $S_2^{\text{HS}}$  signal obtained at cryogenic conditions has a different structure and hence a different barrier for the conversion of the  $S_2^{\text{HS}}$  state into the  $S_2^{\text{LS}}$  state than found here at physiological temperature. Alternatively, the discrepancies to the earlier experimental data are due to species differences.

Since the assignments of the  $W_s$  exchange rates to the  $S_2^{\text{HS}}$  and  $S_2^{\text{LS}}$  states is solid, and the conversion of these rates into energetic barriers is straight forward, we regard our determination of the energetic barrier to be relevant for *T. elongatus* PSII core preparations at physiological temperatures, and to be a strong support for (i) the Mn4 exchange pathway for O5 proposed previously based on DFT calculations,<sup>81</sup> and (ii) the identification of  $W_s$  as O5. It is also in line with the idea that the high pH induced  $S_2^{\text{HS}}$  state has an  $S_2^{\text{AW}}$  like structure,<sup>39,41,43,47</sup> but other water/hydroxide-bound conformations as for example  $S_2^{\text{BW}}$  cannot be excluded.  $S_2^{\text{BW}}$  is similar to intermediate 2A-3 (Scheme 2A), which was calculated to have a total energy 4.6 kcal above  $S_2^{\text{A}}$ ,<sup>81</sup> thus not too far from the level expected for  $S_2^{\text{HS}}$  (Fig. 4). Additional constraints for structure and oxidation states of the  $S_2^{\text{HS}}$  state comes from a recent report of Mino and Nagashima, in which they utilized the orientation dependence of the  $S_2^{\text{HS}}$  EPR signal to identify that (i) Mn4 is the only Mn(III) ion in the  $S_2^{\text{HS}}$  state, and (ii) there needs to be a strong coupling (short distance) between Mn4 and Mn3 to simulate their data within a four-spin coupling scheme.<sup>101</sup>

## Exchange of O5 in the $S_3$ state

For the  $S_3$  state, Siegbahn proposed that water exchange requires the back-donation of one electron from  $Y_Z$  to the  $\text{Mn}_4\text{Ca}$  cluster in order to reduce one of the four Mn(IV) ions to Mn(III),<sup>81</sup> which would allow  $S_2$ -type water exchange. In this  $S_2Y_Z^\bullet$  state, the  $\text{Mn}_4\text{Ca}$  cluster would likely reside in the  $S_2^{\text{AW}}$  structure, and could thus exchange O5 with the rate  $k_i$ . If one then assumes that the transition state for the reduction of the  $\text{Mn}_4\text{Ca}$  cluster by  $Y_Z$  has a similar barrier to the water exchange starting from  $S_2^{\text{A}}$ , this would resolve a major criticism of Siegbahn's Mn4-site exchange proposal for O5. This criticism relates to the experimental finding that, at neutral pH,  $W_s$  exchanges in the  $S_2$  and  $S_3$  states with very similar rates, while the equilibrium between  $S_3Y_Z$  and  $S_2Y_Z^\bullet$  would be expected to slow down the O5 exchange in the  $S_3$  state, given that the  $S_2Y_Z^\bullet$  population must be very low, as this state has not been experimentally observed at neutral pH.

The situation is, however, very different at pH 8.6. Here, the  $S_2Y_Z^\bullet$  state is clearly observed by EPR and hence significantly populated.<sup>102</sup> Thus, one may expect that substrate water exchange in the  $S_3$  state at pH 8.6 should occur fast (with rate  $k_i$ ) in a significant fraction of centers, resulting in a bi-phasic exchange curve as observed in Fig. 2D for the  $S_2$  state. By contrast, a monophasic exchange was observed at high pH for the  $S_3$  state samples (Fig. 3), which occurred with a rate that was 6-fold slower than that in the  $S_2$  state, and also clearly retarded relative to comparable  $S_3$  state data obtained previously at neutral pH,<sup>55,77,103</sup> see also ref. 75.

The recent experimental evidence for the  $S_3^{\text{B}}$  conformation<sup>55</sup> allows proposing an alternative exchange pathway for O5 in the  $S_3$  state. As shown in Scheme 1,  $S_3^{\text{B}}$  may be reached from the dominant  $S_3^{\text{AW}}$  conformation *via*  $S_3^{\text{BW}}$ . After the loss of the O5–water molecule, a new water may bind leading to the re-formation of  $S_3^{\text{AW}}$  containing a new O5.

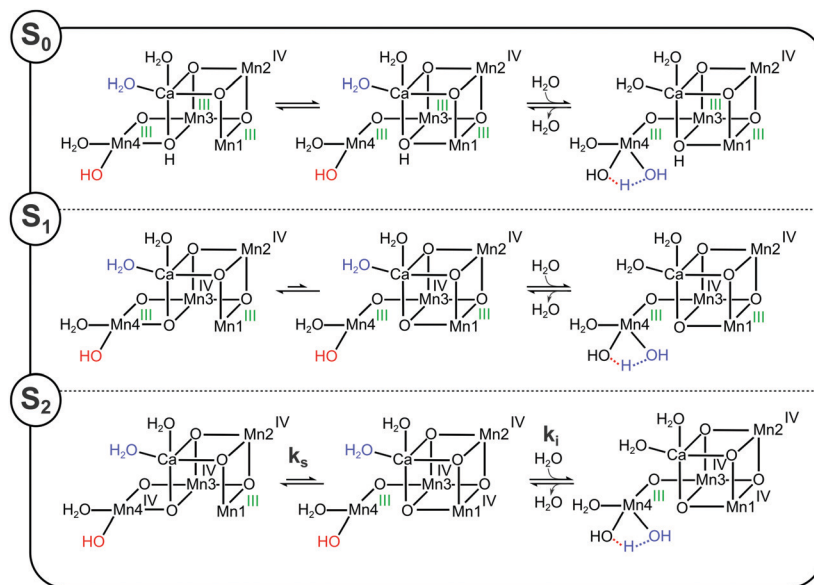
Thus, also the new  $S_3$  state substrate water exchange data are consistent with O5 being the slowly exchanging substrate water  $W_s$ .

## W2 as possible alternative assignment for $W_s$

We evaluated the structures of the  $\text{Mn}_4\text{Ca}$ -cluster to see if  $W_s = \text{O5}$  is the only option to explain our data. One possible alternative was found assuming that the  $S_2^{\text{A}}$  and  $S_2^{\text{B}}$  structures proposed by Pantazis represent the  $S_2^{\text{LS}}$  and  $S_2^{\text{HS}}$  state, respectively.<sup>40</sup> While we presently favor that the  $S_2^{\text{HS}}$  state has a  $S_2^{\text{AW}}$  like structure under our experimental conditions, we discuss this option since it emphasizes the importance of a unique structural resolution of the  $S_2^{\text{HS}}$  state for deriving the mechanism of water oxidation.

Aside from the different position of O5 in the  $S_2^{\text{A}}$  and  $S_2^{\text{B}}$  structures, the major difference between the two  $S_2$  state conformations is the position of the five-coordinate Mn(III) ion. Since a five-coordinate Mn(III) ion should promote rapid water exchange *via* an associative exchange pathway, water ligands bound to the five-coordinate Mn(III) ion in the  $S_2^{\text{HS}}$  state may constitute  $W_s$ . Mn4 has two terminal water derived ligands:





**Scheme 3** Proposed substrate exchange mechanisms for the  $S_0$ ,  $S_1$  and  $S_2$  states assuming that W2 (labelled red) is the slow substrate water and that  $S_2^{\text{HS}}$  has the  $S_2^{\text{B}}$  structure. Mn oxidation states are labelled green for oxidation state III and black for oxidation state IV. In all three S-states the generally more stable  $S_2^{\text{A}}$  conformation (the energy difference in  $S_0$  is proposed to be small) must first convert into the  $S_2^{\text{B}}$  conformation before a water molecule (blue), here suggested to be W3, binds to Mn4. This water donates a proton to W2, which then detaches, after which the  $\text{Mn}_4\text{Ca}$  cluster returns to the  $S_2^{\text{A}}$  conformation with the new water in the W2 position.

W1, which is proposed to bind as fully protonated water molecule hydrogen bonded to D1-Asp61, and W2, which may be bound as a water or hydroxide.<sup>27–30,104</sup> We have previously excluded W1 from being  $W_s$  as it can be replaced by ammonia in the  $S_2$  state with only minor effects on the substrate exchange rates (at pH 7.5).<sup>76</sup> This leaves W2 as a possible alternative candidate for  $W_s$ .

W2, here assumed to be a hydroxide, can be expected to exchange in the  $S_2^{\text{HS}} = S_2^{\text{B}}$  state readily with bulk water (lower panel in Scheme 3) since  $\text{Mn4(III)}$  is placed near the exit of two proposed water channels (O4 and C1 channels) and is also in reach of W3 that is connected to the O1 water channel.<sup>3,105–112</sup> Water exchange in the  $S_2^{\text{LS}} = S_2^{\text{A}}$  state would then occur *via* the equilibrium with the  $S_2^{\text{B}}$  conformation (Scheme 3 and pathway II in Fig. 4).

To scrutinize the alternative W2 proposal, we used the S-state dependence of  $W_s$  exchange. For this, we extended pathway II (Fig. 4) to the other S-states by proposing, in line with previous suggestions,<sup>7,56</sup> as well as experimental data and theoretical calculations,<sup>29,30,38,110,113</sup> that all S-states can exist in A- and B-type conformations, and that the barriers between these conformations are S-state dependent. In addition, we assume that W2, if bound to a non-JT-axis at a six coordinated Mn(III) ion, exchanges much slower as compared to when it is bound to a five-coordinated Mn(III) ion.

In the  $S_0$  state of Ca-PSII, where all Mn ions ligating O5 are in oxidation state (III) and O5 is protonated, the energy difference between the A and B structures and the transition state barrier between them should be small (long arrows of equal length in Scheme 3). Consequently, the  $S_0^{\text{B}}$  form, containing a 5-coordinated  $\text{Mn4(III)}$  site, should be easily attainable, resulting

in the fastest  $W_s$  exchange of all S-states. Consistent with the idea that  $W_s$  exchange occurs in the  $S_0$ ,  $S_1$  and  $S_2$  states at a five-coordinated Mn(III) site, and that the barrier for reaching this state is low in the  $S_0$  state, the rate  $k_s$  in the  $S_0$  state is with about  $10\text{--}20\text{ s}^{-1}$  (in spinach)<sup>75,95</sup> nearly identical to the rate  $k_i$  measured here for the water exchange in the  $S_2^{\text{HS}}$  state (Table 1).

Oxidation of Mn3 during the  $S_0 \rightarrow S_1$  transition strongly stabilizes the  $S_1^{\text{A}}$  state, making it the clearly dominant conformation. Thus, the exchange rate measured for  $W_s$  in the  $S_1$  state, which is about 500 times slower than in the  $S_0$  state, may either reflect the exchange of W2 at the six-coordinated  $\text{Mn4(III)}$  ion, or the barrier for reaching the  $S_1^{\text{B}}$  conformation, in which W2 is bound to a five-coordinated  $\text{Mn4(III)}$  ion facilitating rapid exchange.

Further oxidation of the  $\text{Mn}_4\text{Ca}$  cluster into the  $S_2$  state is expected to increase the exchange rate of W2, since the B-type state can now be stabilized by locating the additional oxidizing equivalent on Mn1. Thus, the barrier for reaching the fast exchanging  $S_2^{\text{B}}$  state can be assumed to be lower than in the  $S_1$  state, explaining the 100-fold faster  $k_s$  exchange rate. In the  $S_3$  state, water exchange can then occur as described above, either by the reduction of the  $\text{Mn}_4\text{Ca}$  into the  $S_2$  state by  $Y_Z$ , or *via* the five-coordinate  $\text{Mn4(IV)}$  site of the  $S_3^{\text{B}}$  state. The main shortcoming of this proposal is the mismatch of the activation barriers described above, that in our view favors the assignment of  $S_2^{\text{HS}}$  to a water/hydroxide bound conformation of the  $S_2$  state, such as  $S_2^{\text{AW}}$ . We anticipate that all the arguments above are exactly the same if W2 were a water molecule instead of a hydroxide.

#### O4 as possible alternative assignment for $W_s$

The  $S_2^{\text{API}}$  structure for the  $S_2^{\text{HS}}$  state involves the protonation of O4. Thus, if O4 were  $W_s$ , this would likely result in a faster



exchange of  $W_s$  in the  $S_2^{HS}$  state as compared to the  $S_2^{LS} = S_2^A$  state. Indeed, O4 was recently suggested to form the O–O bond with an H-bonded water molecule.<sup>69,70</sup> However, we were not able to propose a scheme for the exchange of O4 that appeared consistent with the water exchange data. Additionally, the assignment of  $W_s$  to O4 would be in conflict with the EDNMR assignment of O5 as the only exchangeable oxo bridge of the  $Mn_4Ca$  cluster,<sup>67</sup> and with the recent polarized EPR data of the  $S_2^{HS}$  state.<sup>101</sup>

### The fast exchanging substrate $W_f$

The most significant finding of this study regarding the exchange of  $W_f$  in the  $S_2$  state is the invariance of  $k_f$  towards the substitution of Ca by Sr. This is important, since in recent proposals for the  $S_2 \rightarrow S_3$  transition it is frequently assumed that  $W_3$  is  $W_f$ , which would be bound to Ca in the  $S_0$ ,  $S_1$  and  $S_2$  states, but to Mn1 or Mn4 in the  $S_3$  state. The lack of Ca/Sr dependence in the present  $S_2$  state data thus disfavors that  $W_3$  is a substrate. However, this option cannot be excluded until firm data for the rate of diffusion of substrate water to the catalytic site are obtained. While it generally would be assumed to be unlikely that water access is limiting the fast water exchange, it cannot be excluded *a priori* since present calculations indicate that all channels have barriers in the range of  $10 \text{ kcal mol}^{-1}$ ,<sup>109,114</sup> and a NMR proton relaxation study indicates a distance of  $10 \text{ \AA}$  from the spin center of the  $Mn_4Ca$  cluster to the protons that rapidly exchange with the protons of bulk water.<sup>115</sup>

In case that there are no significant access barriers for  $W_f$  exchange, the previously proposed  $W_2$  assignment remains the best option for  $W_f$ , and the reported low barrier of the  $S_2^A \leftrightarrow S_2^B$  equilibrium may provide the means for fast  $W_2$  exchange (similar to Scheme 3).

Given these presently equally likely options for  $W_f$  (in case  $W_s = O5$ ), detailed mutational studies aiming to increase or decrease the access of water through the known channels connecting the OEC with bulk water will be needed for a final decision. Such experiments are beyond the scope of the present study.

### Possible mechanisms of water oxidation in PSII

The energetics for  $W_s$  exchange determined here for samples in the  $S_2^{LS}$  state agree well with those calculated by Siegbahn for the O5 exchange starting from the  $S_2^A$  state, and thereby strongly support the earlier assignment of  $W_s$  to O5 by Messinger and Siegbahn.<sup>64,66</sup> The present data favor that a  $S_2^{AW}$ -like conformation is both an intermediate in the exchange of O5 and the structure of the  $S_2^{HS}$  state (Fig. 5A). However, in case that the  $S_2^{HS}$  state adopts the closed cubane conformation ( $S_2^B$ ), we are unable to exclude  $W_2$  as the slow substrate water, since a consistent proposal for water exchange could be made for both O5 and  $W_2$  (Fig. 5B and C). For a final assignment further studies will be required, such as  $^{17}\text{O}$ -EDNMR experiments with high-enough time and spectral resolution to allow monitoring the time course of  $^{17}\text{O}/^{16}\text{O}$ -exchange of both  $W_2$  and O5,<sup>67</sup> thus allowing the comparison of the  $W_2$  and O5 exchange rates with

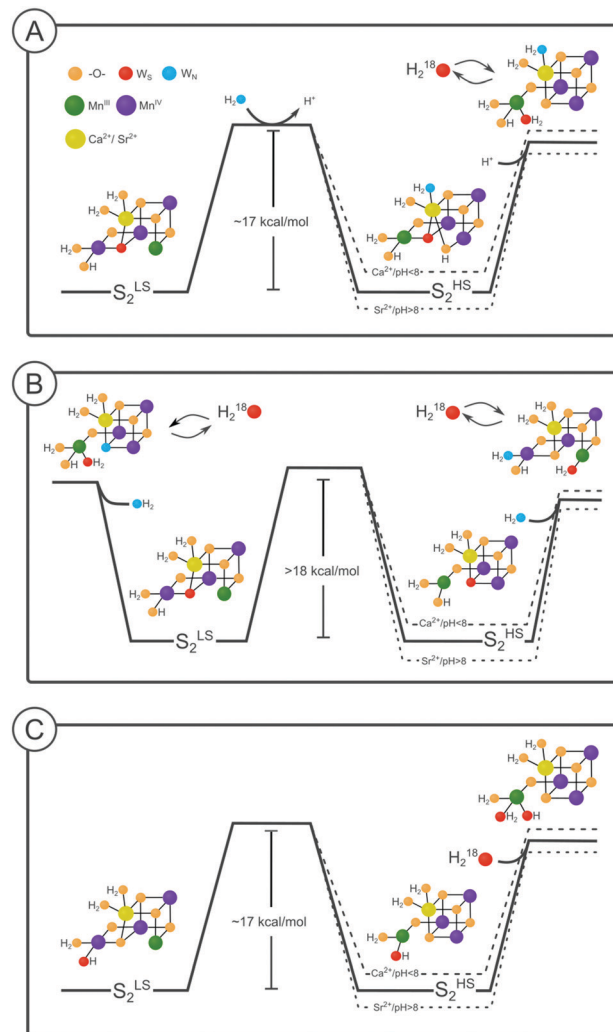


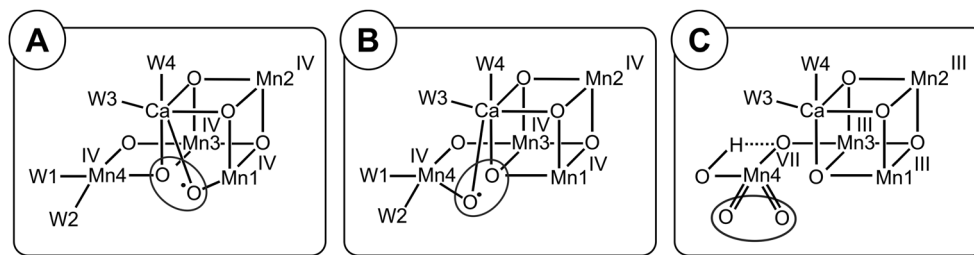
Fig. 5 Possible substrate water exchange pathways in the  $S_2$  state. The energy diagram shown as solid line indicates the case for Sr-PSII at pH 6. Dashed lines indicate changes in the relative energies of  $S_2^{LS}$  and  $S_2^{HS}$  due to pH and/or substitution of Ca by Sr.

those of  $W_s$  determined by TR-MIMS experiments. In addition, obtaining room temperature crystal structures of the high pH  $S_2^{HS}$  state would allow removing the remaining uncertainties. With regard to  $W_f$ , both  $W_2$  and  $W_3$  remain options until the possible role of water accessibility to the catalytic site on the rate of fast water exchange is clarified by mutational studies in combination with substrate water exchange. By contrast, all other options can be excluded.

On that basis, O–O bond formation mechanisms *via* radical coupling involving O5 as  $W_s$  are strongly favored by our new results and may occur in either an A-type or B-type conformation of the  $Mn_4Ca$  cluster (Scheme 4A and B).<sup>7,11,12,63,64,66,85,116,117</sup> The only difference would be that the radical coupling in the  $S_3^{BW}$  state would require first a structural rearrangement starting from  $S_3^{AW}$ , possibly in line with the lag phase observed after the  $S_3Y_Z^\bullet$  formation.<sup>118,119</sup> Interestingly, the origin of the two substrate oxygen's would vary depending on the water insertion pathway.







**Scheme 4** Possible O–O bond formation pathways in photosystem II. (A) A-type radical coupling,<sup>12,65</sup> (B) B-type radical coupling<sup>63,64,85</sup> and (C) geminal coupling at Mn4.<sup>22</sup> For further details, see text.

Assuming that the  $S_2 \rightarrow S_3$  transition would involve W3 binding to Mn1 or Mn4,<sup>3,45,50,120,121</sup> then in both cases the O–O bond would be formed between the former W3 and O5, but the origin of oxygen's in the O5 and Ox/O6 positions would be swapped depending on the insertion site. If, however, water is inserted during the  $S_2 \rightarrow S_3$  transition *via* the pivot mechanism,<sup>32</sup> then mechanisms A and B (Scheme 4) would involve O–O bond formation between W2 and O5.<sup>7,13,64</sup>

By contrast, if Ox/O6 originates from W3, but is not a substrate, W3 would be 'parked' in the  $S_3$  state between Ca and Mn1 to replace O5 during the  $S_3 \rightarrow S_4 \rightarrow S_0$  transition, while the O–O bond would be formed between W2 and O5 *via* geminal coupling at the Mn4 site (Scheme 4C). Geminal coupling at this site was proposed first by Kusunoki on the basis of DFT calculations that resulted in a B-type structure for the  $Mn_4Ca$  cluster.<sup>113</sup> The proposal was further inspired by his analysis of substrate water exchange data from Hillier and Wydrzynski.<sup>60</sup> He suggested that, in the  $S_3$  state, there is a significant correlation between the exchange of  $W_f$  and  $W_s$ , indicating that both must be bound at the same Mn ion to allow them to swap places. At the time the proposal was made, water addition to the  $Mn_4Ca$  cluster during the  $S_2 \rightarrow S_3$  transition was not established, and thus the different S-state dependence of  $W_f$  and  $W_s$  seemed to exclude this idea. In addition, the demonstration that ammonia binds to the W1 site in the  $S_2$  state without significantly affecting the exchange of the two substrate waters argued against this proposal.<sup>76,122</sup>

However, in the light of the recent data suggesting the binding of W3 to Mn1 during  $S_3^{AW}$  formation, geminal coupling is now consistent with present experimental results. Zhang and Sun recently proposed that this type of O–O bond formation involves the transient formation of a  $Mn4(VII)$  species obtained *via* disproportionation within the  $Mn_4Ca$  cluster.<sup>22</sup>

While we cannot yet distinguish between the three options displayed in Scheme 4, we exclude nucleophilic attack of a Ca-bound (W3) water onto W2,<sup>59,65,94,123–126</sup> since W3 would need to serve a dual role: firstly it would need to fill the open coordination site of Mn1 for preloading the new O5, and secondly the successor water ligand at the W3 site would need to be the fast exchanging substrate  $W_f$ . Notably, in case of the pivot pathway for filling the Ox/O6 site, both nucleophilic attack of W3 onto W2, and geminal coupling at the Mn4 site are excluded. Thus clarifying the pathway for water insertion in the  $S_2 \rightarrow S_3$  transition is another requirement for deriving an

experimentally confirmed mechanism. Such studies are ongoing in the field, so that the discussion provided here can serve as blueprint for identifying the substrate once this independent problem is solved.

## Conclusion

Substrate water exchange experiments provide a unique and independent view on the water oxidation mechanism. In this study, we have advanced this approach significantly by providing unique new experimental results. By combining these new data with emerging knowledge about the structures of various conformers of each S-state, together with earlier DFT calculations regarding O5 exchange, we have derived molecular interpretations of substrate water binding and its exchange with bulk water not previously attainable. The present analysis along with future investigations of the temperature dependence for the barrier between LS and HS states, provides the basis for the interpretation of ongoing TR-MIMS experiments utilizing point mutations, Ca/Sr-exchange and H/D-labelling, which together with other outlined experiments have the potential to resolve the mechanism of water oxidation.

## Conflicts of interest

There are no conflicts to declare.

## Acknowledgements

This work was initiated together with Alain Boussac who provided the Ca-PSII and Sr-PSII samples and contributed to the experimental design. We acknowledge the discussions with Vittal Yachandra and Dimitrios Pantazis regarding the nature of the  $S_2^{HS}$  state, and Dmitry Shevela for assistance with graphical representations for this manuscript. Financial support for this project was provided by Vetenskapsrådet (grant number: 2016-05183).

## References

- 1 J.-R. Shen, *Annu. Rev. Plant Biol.*, 2015, **66**, 23–48.
- 2 N. Nelson and W. Junge, *Annu. Rev. Biochem.*, 2015, **84**, 659–683.



- 3 J. Kern, R. Chatterjee, I. D. Young, F. D. Fuller, L. Lassalle, M. Ibrahim, S. Gul, T. Fransson, A. S. Brewster, R. Alonso-Mori, R. Hussein, M. Zhang, L. Douthit, C. de Lichtenberg, M. H. Cheah, D. Shevela, J. Wersig, I. Seuffert, D. Sokaras, E. Pastor, C. Weninger, T. Kroll, R. G. Sierra, P. Aller, A. Butryn, A. M. Orville, M. Liang, A. Batyuk, J. E. Koglin, S. Carbajo, S. Boutet, N. W. Moriarty, J. M. Holton, H. Dobbek, P. D. Adams, U. Bergmann, N. K. Sauter, A. Zouni, J. Messinger, J. Yano and V. K. Yachandra, *Nature*, 2018, **563**, 421–425.
- 4 D. A. Pantazis, *ACS Catal.*, 2018, **8**, 9477–9507.
- 5 W. Junge, *Q. Rev. Biophys.*, 2019, **52**, 1–17.
- 6 B. Kok, B. Forbush and M. McGloin, *Photochem. Photobiol.*, 1970, **11**, 457–475.
- 7 N. Cox and J. Messinger, *Biochim. Biophys. Acta, Bioenerg.*, 2013, **1827**, 1020–1030.
- 8 J. Messinger and G. Renger, in *Primary Processes of Photosynthesis, Part 2*, ed. G. Renger, The Royal Society of Chemistry, Cambridge, UK, 2008, pp. 291–349.
- 9 L. V. Kulik, B. Epel, W. Lubitz and J. Messinger, *J. Am. Chem. Soc.*, 2007, **129**, 13421–13435.
- 10 M. H. Cheah, M. Zhang, D. Shevela, F. Mamedov, A. Zouni and J. Messinger, *Proc. Natl. Acad. Sci. U. S. A.*, 2020, **117**, 141.
- 11 P. E. M. Siegbahn, *Acc. Chem. Res.*, 2009, **42**, 1871–1880.
- 12 N. Cox, D. A. Pantazis, F. Neese and W. Lubitz, *Acc. Chem. Res.*, 2013, **46**, 1588–1596.
- 13 N. Cox, M. Retegan, F. Neese, D. A. Pantazis, A. Boussac and W. Lubitz, *Science*, 2014, **345**, 804–808.
- 14 J. Yano and V. Yachandra, *Chem. Rev.*, 2014, **114**, 4175–4205.
- 15 I. Zaharieva, P. Chernev, G. Berggren, M. Anderlund, S. Styring, H. Dau and M. Haumann, *Biochemistry*, 2016, **55**, 4197–4211.
- 16 M. Askerka, G. W. Brudvig and V. S. Batista, *Acc. Chem. Res.*, 2017, **50**, 41–48.
- 17 N. Schuth, I. Zaharieva, P. Chernev, G. Berggren, M. Anderlund, S. Styring, H. Dau and M. Haumann, *Inorg. Chem.*, 2018, **57**, 10424–10430.
- 18 H. Dau, L. Iuzzolino and J. Dittmer, *Biochim. Biophys. Acta, Bioenerg.*, 2001, **1503**, 24–39.
- 19 M. Haumann, C. Müller, P. Liebisch, L. Iuzzolino, J. Dittmer, M. Grabolle, T. Neisius, W. Meyer-Klaucke and H. Dau, *Biochemistry*, 2005, **44**, 1894–1908.
- 20 W. Hillier and J. Messinger, in *Photosystem II: The Light-Driven Water:Plastoquinone Oxidoreductase*, ed. T. J. Wydrzynski, K. Satoh and J. A. Freeman, Springer, Netherlands, Dordrecht, 2005, pp. 567–608.
- 21 J. P. McEvoy and G. W. Brudvig, *Chem. Rev.*, 2006, **106**, 4455–4483.
- 22 B. Zhang and L. Sun, *Dalton Trans.*, 2018, **47**, 14381–14387.
- 23 Y. Umena, K. Kawakami, J.-R. Shen and N. Kamiya, *Nature*, 2011, **473**, 55–60.
- 24 M. Suga, F. Akita, K. Hirata, G. Ueno, H. Murakami, Y. Nakajima, T. Shimizu, K. Yamashita, M. Yamamoto, H. Ago and J.-r. Shen, *Nature*, 2014, **517**, 99–103.
- 25 M. Suga, F. Akita, K. Yamashita, Y. Nakajima, G. Ueno, H. Li, T. Yamane, K. Hirata, Y. Umena, S. Yonekura, L.-J. Yu, H. Murakami, T. Nomura, T. Kimura, M. Kubo, S. Baba, T. Kumasaka, K. Tono, M. Yabashi, H. Isobe, K. Yamaguchi, M. Yamamoto, H. Ago and J.-R. Shen, *Science*, 2019, **366**, 334.
- 26 J. H. Robblee, J. Messinger, R. M. Cinco, K. L. McFarlane, C. Fernandez, S. A. Pizarro, K. Sauer and V. K. Yachandra, *J. Am. Chem. Soc.*, 2002, **124**, 7459–7471.
- 27 V. Krewald, M. Retegan, N. Cox, J. Messinger, W. Lubitz, S. DeBeer, F. Neese and D. A. Pantazis, *Chem. Sci.*, 2015, **6**, 1676–1695.
- 28 S. Nakamura and T. Noguchi, *Proc. Natl. Acad. Sci. U. S. A.*, 2016, 201607897, DOI: 10.1073/pnas.1607897113.
- 29 D. Narzi, G. Mattioli, D. Bovi and L. Guidoni, *Chem. – Eur. J.*, 2017, **23**, 6969–6973.
- 30 K. Miyagawa, H. Isobe, T. Kawakami, M. Shoji, S. Yamanaka, M. Okumura, T. Nakajima and K. Yamaguchi, *Chem. Phys. Lett.*, 2019, **734**, 136731.
- 31 J. Yano, J. Kern, K. Sauer, M. J. Latimer, Y. Pushkar, J. Biesiadka, B. Loll, W. Saenger, J. Messinger, A. Zouni and V. K. Yachandra, *Science*, 2006, **314**, 821–825.
- 32 M. Retegan, V. Krewald, F. Mamedov, F. Neese, W. Lubitz, N. Cox and D. A. Pantazis, *Chem. Sci.*, 2016, **7**, 72–84.
- 33 G. C. Dismukes and Y. Siderer, *Proc. Natl. Acad. Sci. U. S. A.*, 1981, **78**, 274–278.
- 34 J. L. Casey and K. Sauer, *Biochim. Biophys. Acta, Bioenerg.*, 1984, **767**, 21–28.
- 35 J. L. Zimmermann and A. W. Rutherford, *Biochemistry*, 1986, **25**, 4609–4615.
- 36 A. Boussac, J. J. Girerd and A. W. Rutherford, *Biochemistry*, 1996, **35**, 6984–6989.
- 37 T. S. Kuntzleman and A. Haddy, *Photosynth. Res.*, 2009, **102**, 7.
- 38 A. Boussac, I. Ugur, A. Marion, M. Sugiura, V. R. I. Kaila and A. W. Rutherford, *Biochim. Biophys. Acta, Bioenerg.*, 2018, **1859**, 342–356.
- 39 A. Boussac, *Biochim. Biophys. Acta, Bioenerg.*, 2019, **1860**, 508–518.
- 40 D. A. Pantazis, W. Ames, N. Cox, W. Lubitz and F. Neese, *Angew. Chem., Int. Ed.*, 2012, **51**, 9935–9940.
- 41 P. E. M. Siegbahn, *Phys. Chem. Chem. Phys.*, 2018, **20**, 22926–22931.
- 42 T. A. Corry and P. J. O'Malley, *J. Phys. Chem. Lett.*, 2019, 5226–5230.
- 43 Y. Pushkar, A. K. Ravari, S. C. Jensen and M. Palenik, *J. Phys. Chem. Lett.*, 2019, **10**, 5284–5291.
- 44 G. Renger, *Photosynthetica*, 1987, **21**, 203–224.
- 45 D. Bovi, D. Narzi and L. Guidoni, *Angew. Chem., Int. Ed.*, 2013, **52**, 11744–11749.
- 46 H. Isobe, M. Shoji, S. Yamanaka, Y. Umena, K. Kawakami, N. Kamiya, J.-R. Shen and K. Yamaguchi, *Dalton Trans.*, 2012, **41**, 13727.
- 47 R. Chatterjee, G. Han, J. Kern, S. Gul, F. D. Fuller, A. Garachtchenko, I. D. Young, T.-C. Weng, D. Nordlund, R. Alonso-Mori, U. Bergmann, D. Sokaras, M. Hatakeyama,



- V. K. Yachandra and J. Yano, *Chem. Sci.*, 2016, **7**, 5236–5248.
- 48 R. Chatterjee, L. Lassalle, S. Gul, F. D. Fuller, I. D. Young, M. Ibrahim, C. de Lichtenberg, M. H. Cheah, A. Zouni, J. Messinger, V. K. Yachandra, J. Kern and J. Yano, *Physiol. Plant.*, 2019, **166**, 60–72.
- 49 M. Askerka, D. J. Vinyard, G. W. Brudvig and V. S. Batista, *Biochemistry*, 2015, **54**, 5783–5786.
- 50 I. Ugur, A. W. Rutherford and V. R. I. Kaila, *Biochim. Biophys. Acta, Bioenerg.*, 2016, **1857**, 740–748.
- 51 N. Ioannidis and V. Petrouleas, *Biochemistry*, 2000, **39**, 5246–5254.
- 52 V. Petrouleas, D. Koulougliotis and N. Ioannidis, *Biochemistry*, 2005, **44**, 6723–6728.
- 53 K. G. V. Havelius, J.-H. Su, Y. Feyziyev, F. Mamedov and S. Styring, *Biochemistry*, 2006, **45**, 11.
- 54 A. Boussac, M. Sugiura, T.-L. Lai and A. W. Rutherford, *Philos. Trans. R. Soc., B*, 2008, **363**, 1203–1210.
- 55 M. Chrysina, E. Heyno, Y. Kutin, M. Reus, H. Nilsson, M. M. Nowaczyk, S. DeBeer, F. Neese, J. Messinger, W. Lubitz and N. Cox, *Proc. Natl. Acad. Sci. U. S. A.*, 2019, **166**, 6.
- 56 G. Renger, *Biochim. Biophys. Acta, Bioenerg.*, 2012, **1817**, 1164–1176.
- 57 H. Isobe, M. Shoji, J. R. Shen and K. Yamaguchi, *Inorg. Chem.*, 2016, **55**, 502–511.
- 58 T. A. Corry and P. J. O'Malley, *J. Phys. Chem. Lett.*, 2018, **9**, 6269–6274.
- 59 J. Messinger, M. Badger and T. Wydrzynski, *Proc. Natl. Acad. Sci. U. S. A.*, 1995, **92**, 3209–3213.
- 60 W. Hillier and T. Wydrzynski, *Coord. Chem. Rev.*, 2008, **252**, 306–317.
- 61 G. Hendry and T. Wydrzynski, *Biochemistry*, 2003, **42**, 6209–6217.
- 62 W. Hillier, J. Messinger and T. Wydrzynski, *Biochemistry*, 1998, **37**, 16908–16914.
- 63 H. Nilsson, T. Krupnik, J. Kargul and J. Messinger, *Biochim. Biophys. Acta, Bioenerg.*, 2014, **1837**, 1257–1262.
- 64 J. Messinger, *Phys. Chem. Chem. Phys.*, 2004, **6**, 4764–4771.
- 65 K. N. Ferreira, T. M. Iverson, K. Maghlaoui, J. Barber and S. Iwata, *Science*, 2004, **303**, 1831–1838.
- 66 P. E. M. Siegbahn, *Chem. – Eur. J.*, 2006, **12**, 9217–9227.
- 67 L. Rapatskiy, N. Cox, A. Savitsky, W. M. Ames, J. Sander, M. M. Nowaczyk, M. Rögner, A. Boussac, F. Neese, J. Messinger and W. Lubitz, *J. Am. Chem. Soc.*, 2012, **134**, 16619–16634.
- 68 D. J. Vinyard, S. Khan and G. W. Brudvig, *Faraday Discuss.*, 2015, **185**, 37–50.
- 69 M. Suga, F. Akita, M. Sugahara, M. Kubo, Y. Nakajima, T. Nakane, K. Yamashita, Y. Umena, M. Nakabayashi, T. Yamane, T. Nakano, M. Suzuki, T. Masuda, S. Inoue, T. Kimura, T. Nomura, S. Yonekura, L.-J. Yu, T. Sakamoto, T. Motomura, J.-H. Chen, Y. Kato, T. Noguchi, K. Tono, Y. Joti, T. Kameshima, T. Hatsui, E. Nango, R. Tanaka, H. Naitow, Y. Matsuura, A. Yamashita, M. Yamamoto, O. Nureki, M. Yabashi, T. Ishikawa, S. Iwata and J.-R. Shen, *Nature*, 2017, **543**, 131–135.
- 70 K. Kawashima, T. Takaoka, H. Kimura, K. Saito and H. Ishikita, *Nat. Commun.*, 2018, **9**, 1247.
- 71 M. Sugiura and Y. Inoue, *Plant Cell Physiol.*, 1999, **40**, 1219–1231.
- 72 M. Sugiura, A. Boussac, T. Noguchi and F. Rappaport, *Biochim. Biophys. Acta, Bioenerg.*, 2008, **1777**, 331–342.
- 73 N. Ishida, M. Sugiura, F. Rappaport, T.-L. Lai, A. W. Rutherford and A. Boussac, *J. Biol. Chem.*, 2008, **283**, 13330–13340.
- 74 M. Sugiura, Y. Ozaki, M. Nakamura, N. Cox, F. Rappaport and A. Boussac, *Biochim. Biophys. Acta, Bioenerg.*, 2014, **1837**, 1922–1931.
- 75 W. Hillier and T. Wydrzynski, *Phys. Chem. Chem. Phys.*, 2004, **6**, 4882–4889.
- 76 M. Perez Navarro, W. M. Ames, H. Nilsson, T. Lohmiller, D. A. Pantazis, L. Rapatskiy, M. M. Nowaczyk, F. Neese, A. Boussac, J. Messinger, W. Lubitz and N. Cox, *Proc. Natl. Acad. Sci. U. S. A.*, 2013, **110**, 15561–15566.
- 77 H. Nilsson, F. Rappaport, A. Boussac and J. Messinger, *Nat. Commun.*, 2014, **5**, 1–7.
- 78 W. Hillier, I. McConnell, S. Singh, R. Debus, A. Boussac and T. Wydrzynski, *Photosynthesis. Energy from the Sun: 14th International Congress on Photosynthesis*, Springer, Dordrecht, 2008, pp. 427–430.
- 79 F. Pitari, D. Bovi, D. Narzi and L. Guidoni, *Biochemistry*, 2015, **54**, 5959–5968.
- 80 D. J. Vinyard, S. Khan, M. Askerka, V. S. Batista and G. W. Brudvig, *J. Phys. Chem. B*, 2017, **121**, 1020–1025.
- 81 P. E. M. Siegbahn, *J. Am. Chem. Soc.*, 2013, **135**, 9442–9449.
- 82 W. F. Beck, J. C. De Paula and G. W. Brudvig, *J. Am. Chem. Soc.*, 1986, **108**, 4018–4022.
- 83 R. D. Britt, J.-L. Zimmermann, K. Sauer and M. P. Klein, *J. Am. Chem. Soc.*, 1989, **111**, 3522–3532.
- 84 M. C. W. Evans, R. J. Ball and J. H. A. Nugent, *FEBS Lett.*, 2005, **579**, 3081–3084.
- 85 X. Li and P. E. M. Siegbahn, *Phys. Chem. Chem. Phys.*, 2015, **17**, 12168–12174.
- 86 M. Shoji, H. Isobe, Y. Shigeta, T. Nakajima and K. Yamaguchi, *J. Phys. Chem. B*, 2018, **122**, 6491–6502.
- 87 M. Shoji, H. Isobe and K. Yamaguchi, *Chem. Phys. Lett.*, 2019, **714**, 219–226.
- 88 W. Hillier and T. Wydrzynski, *Biochemistry*, 2000, **39**, 4399–4405.
- 89 W. Hillier and T. Wydrzynski, *Biochim. Biophys. Acta, Bioenerg.*, 2001, **1503**, 197–209.
- 90 M. Lundberg, M. R. A. Blomberg and P. E. M. Siegbahn, *Theor. Chem. Acc.*, 2003, **110**, 130–143.
- 91 L. Helm and A. E. Merbach, *Chem. Rev.*, 2005, **105**, 1923–1960.
- 92 R. Tagore, H. Chen, R. H. Crabtree and G. W. Brudvig, *J. Am. Chem. Soc.*, 2006, **128**, 9457–9465.
- 93 R. Tagore, R. H. Crabtree and G. W. Brudvig, *Inorg. Chem.*, 2007, **46**, 2193–2203.
- 94 E. M. Sproviero, M. B. Newcomer, J. A. Gascón, E. R. Batista, G. W. Brudvig and V. S. Batista, *Photosynth. Res.*, 2009, **102**, 455–470.



- 95 W. Hillier and T. Wydrzynski, *Biochemistry*, 2000, **39**, 4399–4405.
- 96 M. Capone, D. Bovi, D. Narzi and L. Guidoni, *Biochemistry*, 2015, **54**, 6439–6442.
- 97 M. Shoji, H. Isobe and K. Yamaguchi, *Chem. Phys. Lett.*, 2015, **636**, 172–179.
- 98 M. Askerka, J. Wang, D. J. Vinyard, G. W. Brudvig and V. S. Batista, *Biochemistry*, 2016, **55**, 981–984.
- 99 M. Capone, D. Narzi, D. Bovi and L. Guidoni, *J. Phys. Chem. Lett.*, 2016, **7**, 592–596.
- 100 J. C. de Paula, W. F. Beck, A.-F. Miller, R. B. Wilson and G. W. Brudvig, *J. Chem. Soc., Faraday Trans. 1*, 1987, **83**, 3635–3651.
- 101 H. Mino and H. Nagashima, *J. Phys. Chem. B*, 2020, **124**, 128–133.
- 102 P. Geijer, F. Morvaridi and S. Styring, *Biochemistry*, 2001, **40**, 10881–10891.
- 103 W. Hillier, I. Mcconnell, S. Singh, R. Debus, A. Boussac and T. Wydrzynski, *Photosynthesis. Energy from the Sun: 14th International Congress on Photosynthesis*, Springer, Dordrecht, 2008, pp. 427–430.
- 104 W. Ames, D. A. Pantazis, V. Krewald, N. Cox, J. Messinger, W. Lubitz and F. Neese, *J. Am. Chem. Soc.*, 2011, **133**, 19743–19757.
- 105 J. W. Murray and J. Barber, *J. Struct. Biol.*, 2007, **159**, 228–237.
- 106 F. M. Ho and S. Styring, *Biochim. Biophys. Acta, Bioenerg.*, 2008, **1777**, 140–153.
- 107 F. M. Ho, *Photosynth. Res.*, 2008, **98**, 503–522.
- 108 J. W. Murray, K. Maghlaoui, J. Kargul, M. Sugiura and J. Barber, *Photosynth. Res.*, 2008, **98**, 523–527.
- 109 S. Vassiliev, T. Zaraiskaya and D. Bruce, *Biochim. Biophys. Acta, Bioenerg.*, 2012, **1817**, 1671–1678.
- 110 M. Shoji, H. Isobe, S. Yamanaka, Y. Umena, K. Kawakami, N. Kamiya, J.-R. Shen, T. Nakajima and K. Yamaguchi, *Adv. Quantum Chem.*, 2015, **70**, 325–413.
- 111 M. Retegan and D. A. Pantazis, *Chem. Sci.*, 2016, **7**, 6463–6476.
- 112 M. Retegan and D. A. Pantazis, *J. Am. Chem. Soc.*, 2017, **139**, 14340–14343.
- 113 M. Kusunoki, *J. Photochem. Photobiol., B*, 2011, **104**, 100–110.
- 114 S. Vassiliev, T. Zaraiskaya and D. Bruce, *Biochim. Biophys. Acta, Bioenerg.*, 2013, **1827**, 1148–1155.
- 115 G. Han, Y. Huang, F. H. M. Koua, J.-R. Shen, P.-O. Westlund and J. Messinger, *Phys. Chem. Chem. Phys.*, 2014, **16**, 11924.
- 116 P. E. M. Siegbahn, *J. Photochem. Photobiol., B*, 2011, **104**, 94–99.
- 117 P. E. M. Siegbahn, *Biochim. Biophys. Acta, Bioenerg.*, 2013, **1827**, 1003–1019.
- 118 F. Rappaport, M. Blanchard-Desce and J. Lavergne, *Biochim. Biophys. Acta, Bioenerg.*, 1994, **1184**, 178–192.
- 119 M. Haumann, P. Liebisch, C. Müller, M. Barra, M. Grabolle and H. Dau, *Science*, 2005, **310**, 1019.
- 120 C. J. Kim and R. J. Debus, *Biochemistry*, 2017, **56**, 2558–2570.
- 121 H. Sakamoto, T. Shimizu, R. Nagao and T. Noguchi, *J. Am. Chem. Soc.*, 2017, **139**, 2022–2029.
- 122 P. H. Oyala, T. A. Stich, R. J. Debus and R. D. Britt, *J. Am. Chem. Soc.*, 2015, **137**, 8829–8837.
- 123 V. L. Pecoraro, M. J. Baldwin, M. T. Caudle, W.-Y. Hsieh and N. A. Law, *Pure Appl. Chem.*, 1998, **70**, 925–929.
- 124 E. M. Siegbahn and R. H. Crabtree, *J. Am. Chem. Soc.*, 1999, **121**, 10.
- 125 J. S. Vrettos, J. Limburg and G. W. Brudvig, *Biochim. Biophys. Acta, Bioenerg.*, 2001, **1503**, 229–245.
- 126 J. Barber, *Q. Rev. Biophys.*, 2016, **49**, 1–21.

